UNIVERSITA' DEGLI STUDI DI TORINO

Doctoral School in Life and Health Sciences

PhD in Medical Pathophysiology

XXXVII CYCLE

In vitro characterization of 3D culture-based differentiation of human liver stem cells

PhD Thesis – Academic Year 2024-2025

Tutor:

Professor Stefania Bruno

Co-tutor:

Dr. Maria Beatriz Herrera Sanchez, PhD

PhD candidate:

Gabriele Saccu

Abstract

A shortage of functional hepatocytes hampers drug safety testing and therapeutic applications because mature hepatocytes cannot be expanded and tend to lose functionality *in vitro*. Previous studies indicated that human liver stem cells (HLSCs) can differentiate into hepatocyte-like cells in an *in vitro* rotary cell culture system (RCCS), in the presence of different combinations of cytokines and molecules known to play a role in hepatocyte maturation. To characterize the hepatocyte-like cells obtained after HLSC differentiation, we analyzed the expression of stem and hepatic markers by qRT-PCR and immunofluorescence and developed an updated Indocyanine green *in vitro* assay to measure hepatocyte functionality. Our results demonstrated that HLSCs, after one day of differentiation significantly upregulated the expression of hepatic genes, such as CYP 450, urea cycle enzymes and uptake transporters exclusively expressed on the sinusoidal side of mature hepatocytes. In addition, during differentiation, it has been observed a downregulation of stem cell markers, such as Klf4. Further analysis showed that the differentiated cells were able to release urea and FVIII into the supernatant, as early as in the first 24 hours which accumulate over time. In conclusion, the results suggested that the three-dimensional RCCS may promote the rapid hepatic differentiation of HLSCs. Despite the limitations of this rotary culture system, it possesses unique advantages and in addition may provide a potential strategy to characterize HLSCs GMP batches for clinical application.

Table of contents

Introduction *4*

Hematopoietic stem cell **7**

Mesenchymal stromal cells **7**

Human Liver Stem Cell **8**

In vitro hepatocyte-like cells differentiation **10**

Hepatocyte-like cells 3D culture-based differentiation **12**

Aim of the work *14*

Material and Methods *15*

Cell culture **15**

Fluorescence-activated cell sorter (FACS) analysis **15**

In vitro 3D-rotary cell culture system (RCCS) cell differentiation into hepatic lineage **16**

Immunofluorescence staining **16**

Terminal dUTP nick end-labeling (TUNEL) assay **17**

Periodic acid Schiff staining **17**

Western blot **18**

Urea quantification by HPLC-MS/MS and QuantiChrom™ Urea Assay analysis **23**

Statistical analysis **24**

Results *25*

HLSC characterization cultured in 2D condition **25**

Characterization of HLSC aggregates in rotary cell culture system **26**

Differential gene expression analysis by PCR array **28**

Immunofluorescence and RT-PCR analysis of hepatocyte-like differentiated HLSCs **29**

Expression of coagulation factor **31**

Induction of urea metabolism in HLSCs differentiate hepatocyte-like cells. **32**

Stem cell marker modulation of hepatocyte-like HLSCs differentiated in RCCS **35**

Indocyanine green (ICG) uptake by hepatocyte-like HLSCs differentiated in RCCS **36**

Discussion *39*

Conclusions *43*

Future prospective *43*

Abbreviation *45*

Appendix 1 ..... *47*

Appendix 2 ..... *54*

Abroad Period *54*

References *64*

Acknowledgements *72*

Introduction

Liver disease account the 4% of all death due to an acute liver failure (ALF) and may cause progressive end-stage liver disease (ESLD) with an increasing needed of demand for liver transplants [1]. ALF is a rapid and severe deterioration in liver function, typically occurring within days or weeks in individuals with no prior liver disease. Common causes include viral hepatitis, drug-induced liver injury (especially due to acetaminophen overdose), autoimmune liver diseases, and exposure to toxins. ALF is characterized by the liver's inability to detoxify and produce essential proteins, leading to potentially life-threatening complications [2].

ESLD is the final phase of chronic liver conditions, in which the liver sustains such extensive damaged that it can no longer fulfill vital functions, including detoxification, bile production, and protein synthesis. Mortality is largely attributable to complications from cirrhosis, which is often classified into stages of progression: (1) inflammation and fat accumulation (2) fibrosis; (3) cirrhosis; and (4) ESLD or liver cancer. Both ALF and ESLD constitute medical emergencies, often requiring intensive care, and in severe cases, liver transplantation to prevent multi-organ failure and death (Figure1) [1,2].

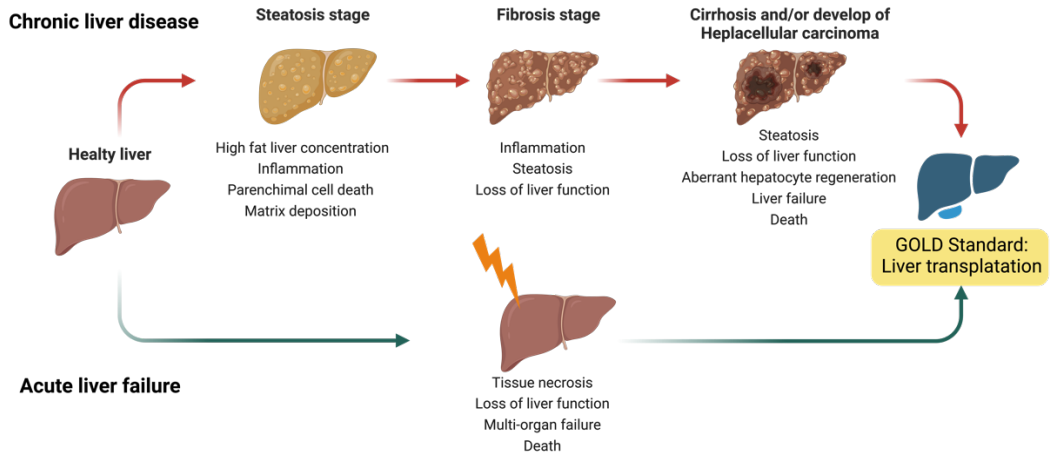

Figure 1: Pathophysiological features and principal key events which lead to clinical transplantation in liver diseases. The upper panel represents the schematic transition of chronic liver disease that develop final cirrhosis and/or hepatocellular carcinoma. The bottom panel represent acute liver failure features. Created with Biorender.com.

However, the limited availability of donors, high costs, risk of organ rejection, potential post-operative complications, and the need for lifelong immunosuppression have driven the development of alternative treatments, such as cell therapy, which has emerged as a key player in regenerative medicine [3]. Cell-based therapies, particularly those utilizing stem cells, offer promising new options for patients with otherwise incurable diseases, shifting the focus from managing symptoms to potentially achieving a cure [4].

To address the shortage of liver donors, hepatocytes have been extensively studied as a primary cell-based therapy for liver diseases. Despite their potential, human hepatocyte transplantation faces significant challenges in clinical application, including limited capacity for *in vitro* expansion, rapid functional decline, and considerable viability loss following cryopreservation. Additionally, the scarcity of liver tissue donors limits the availability of hepatocytes needed for effective patient treatments. Recently, stem cells have gained attention as a promising alternative, with efforts focused on generating mature hepatocytes for therapeutic use [5]. Stem cell therapy, a keystone of regenerative medicine, seeks to enhance the body's intrinsic repair mechanism by stimulating, modulating, and managing endogenous stem cell populations or by replenishing cellular reservoirs. This approach aims to restore tissue homeostasis and facilitate regeneration [4] (Figure 2).

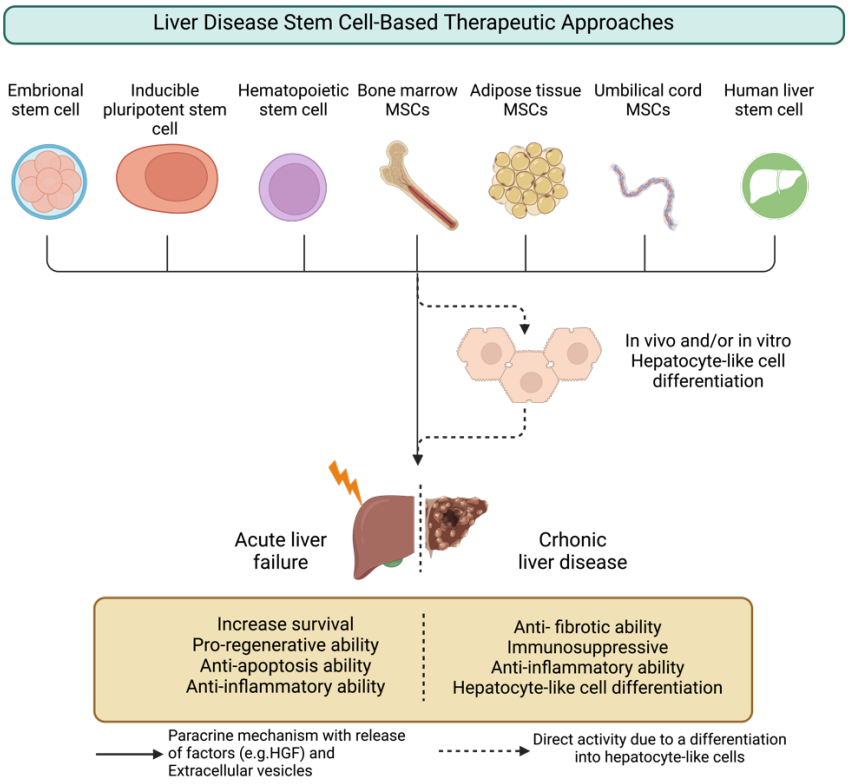

Figure 2: Methods of regenerative medicine for the cell therapy in liver diseases. Schematic representation of the different stem cell source adopted in liver diseases. The therapeutic effect may be achieved using the stem cell paracrine ability. Moreover, *in vitro* or *in vivo* hepatocyte-like differentiation may contribute to liver function and structure regeneration. Created with Biorender.com.

Recent Phase I and II clinical trials have intensified interest in stem cells therapy as a potential treatment for liver fibrosis and cirrhosis, offering hope for reversing these conditions [5,6]. Among the various stem cell types, embryonic stem cells (ESCs) are a promising source, but are limited by significant ethical concerns [7]. An alternative approach uses induced pluripotent stem cells (iPSCs), which are derived from genetically reprogrammed autologous cells such as fibroblasts, and exhibit self-renewal, *in vitro* expansion, and hepatic differentiation capabilities. This makes iPSCs a highly promising source for producing large quantities of functional hepatocyte-like cells [8]. Despite their promise, the generation of iPSC remains both time-consuming and costly, presenting hurdles for clinical application. Additionally, critical aspects such as long-term safety, tolerability, efficacy, and the risk of tumorigenic most be evaluated in future clinical trials to establish their therapeutic viability [9].

Hematopoietic stem cell

Bone marrow CD34 and/or CD133 hematopoietic stem cells (HSCs) have emerged as a promising source of liver-repopulating cells, contributing to liver regeneration after injury. One reported mechanism involved the differentiation of these cells into non-hematopoietic cell types, including hepatocytes [10-12]. Mobilization of HSCs using granulocyte-colony stimulating factor (G-CSF) has also shown promise as a therapeutic strategy, with positive outcomes reported in both animal models and clinical trials. For instance, autologous mobilized $CD34^+$ HSCs have demonstrated the potential to support liver recovery in patients with Alcoholic liver cirrhosis [13]. Furthermore, in patients with hepatitis B virus-related liver cirrhosis, G-CSF combined with peripheral blood mononuclear cells infusion led to greater and more sustained clinical and biochemical improvements [14]. While HSCs may contribute to liver cell repopulation through trans-differentiation, their regenerative effects are largely attributed to the stimulation of liver progenitor cells via paracrine signaling mechanism [15]. Overall, HSC mobilization has shown a favorable safety profile and the potential to improve liver function and survival rates in patients with liver disease. However, further research is needed to optimize and validate this approach to confirm its therapeutic efficacy.

Mesenchymal stromal cells

Mesenchymal stromal cells (MSCs) are adult stem cells extensively investigated and widely used in pre-clinical models of both acute and chronic liver diseases [16]. MSCs can be easily isolated from different tissues, including bone marrow, adipose tissue, umbilical cord, and can be expanded on a large-scale while maintaining a stable phenotype across multiple culture passages [17]. These cells exhibit self-renewal ability and multiple-lineages differentiation capabilities, such as adipocytes, osteoblasts, chondroblasts, and hepatocyte-like cells (HLCs) [18]. In addition, MSCs have demonstrated anti-inflammatory effects, anti-apoptotic properties, immunosuppression activity, pro angiogenetic characteristic, tissue repair promotion, and growth factor production, making them valuable in pre-clinical models of liver diseases [19,20].

Interestingly, the MSC secretome, comprising soluble proteins, cytokines (e.g., IL-10), chemokines, growth factors, such as hepatocyte growth factor (HGF) and Vascular endothelial growth factor (VEGF) , proteases, and extracellular vesicles, has demonstrated regenerative potential for liver repair, including anti-apoptotic and pro-proliferative effects in both *in vitro* and *in vivo* liver disease models [21]. The secretome has shown the ability to modulate immune responses and reduce fibrosis in chronic liver disease settings. Overall, MSCs circumvent some of the critical challenges typically encountered in human clinical trials with ESCs, such as ethical issues, rejection risks, and teratoma formation, positioning them as a highly promising therapeutic avenue for liver disease [17].

Human Liver Stem Cell

In 2006, Herrera et al. isolated and characterized a stem cell-like population within the liver, referred to as human liver stem cells (HLSCs) [22]. Cultivated under controlled *in vitro* conditions, HLSCs exhibited multipotent properties similar to MSCs. Moreover, HLSCs express MSC markers such as CD29, CD73, CD105, CD44, and CD90, while lacking hematopoietic markers (CD34, CD45, CD14), HLA class II, and costimulatory molecules (CD40, CD80, and CD86) [22] [23]. HLSCs also express embryonic stem cell markers like Oct3/4, Nanog, Sox2, and Klf4, along with self-renewal markers SSEA4 and Musashi1, confirming their multipotency [22]. Interestingly, HLSCs co-express liver - specific markers such as albumin (ALB), cytokeratin-(CK)8, alpha-fetoprotein (α-FP) and hepatocyte nuclear factor 4 (HNF4) suggesting their hepatic lineage origin and partial differentiation commitment [22]. (Figure 3).

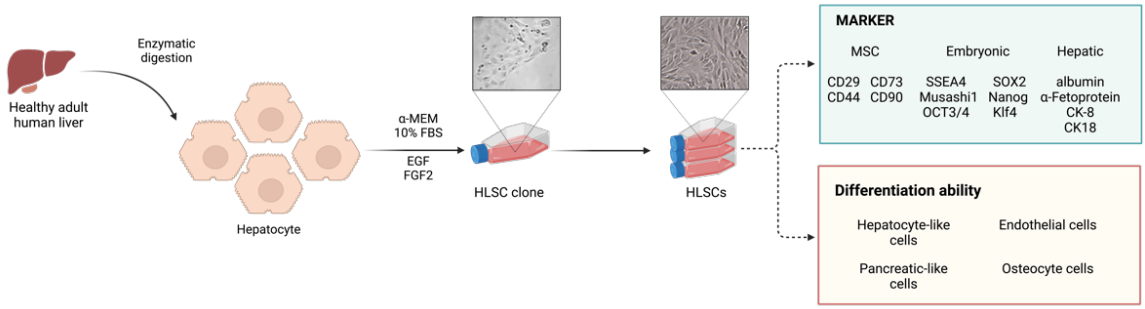

Figure 3: Isolation and characterization process of Human liver stem cells population from healthy liver tissue. Created with Biorender.com.

Our research group has demonstrated the regenerative potential of HLSCs in various liver disease models. In an acute liver injury (ALI) model induced by N-acetyl-p-aminophen, HLSCs injections facilitated liver regeneration [22]. Moreover, HLSCs improved liver regeneration and function in a mouse model of fulminant liver failure (FLF) induced by D-galactosamine and lipopolysaccharide [24], where CK-8 and CK-18 co-expression with HLA suggested HLSCs differentiation into hepatocyte-like cells [24]. Likewise, HLSCs have shown therapeutic potential in a non-alcoholic steatohepatitis (NASH) model, where they reduced fibrosis and ameliorate inflammation [25]. Further studies on HLSCs-based therapies using conditioned media and extracellular vesicles have highlighted their regenerative potential in both acute and chronic liver disease models [24,26]. In particular, HLSC- conditioned media, containing cytokines such as HGF, VEGF, interleukin (IL) 6 and 8, have showed liver regenerative effects comparable to HLSC cell therapy in a mouse model of FLF [24]. In a non-alcoholic steatohepatitis (NASH) mouse model, HLSCs-derived extracellular vesicles displayed anti-fibrotic and anti-inflammatory effects, reducing hepatic stellate cell activation and improving liver function [26].

HLSCs also have immunomodulatory properties that may reduce the risk of transplant rejection [23]. Similar to MSCs, HLSCs inhibit T cell proliferation, dendritic cell differentiation, and natural killer cell degranulation, protecting them from allogeneic lysis [23]. In addition to preclinical *in vivo* studies, the first human Phase I clinical trial of HLSC intra-hepatic administrated in infants with inherited neonatal-onset hyperammonemia, demonstrated the safety of HLSC treatment, with no local or systemic adverse effects observed, and without the need for immunosuppression [27]. This trial marks a promising advancement in the clinical potential of HLSCs for treating inherited liver disorders.

In vitro hepatocyte-like cells differentiation

Liver development in embryos is a complex process involving intricate steps that ultimately lead to the formation of the liver bud from endoderm. During this process, the posterior foregut generates hepatic progenitor cells with the potential to differentiate into both hepatocytes and bile duct cells [28,29]. This differentiation is orchestrated by signaling factors secreted by the mesoderm, including WNT, bone morphogenetic protein (BMP), hepatocyte growth factor (HGF), and fibroblast growth factor (FGF) [30]. The balance of these factors is crucial for hepatic tissue maturation. Notably, the foregut secretes WNT antagonists during hepatocyte development, while the mesoderm surrounding the midgut and hindgut expresses higher levels of WNT and FGF, facilitating the formation of a hepatic diverticulum [28,29]. This process is further aided by the subsequent secretion of FGF from the septum transversum and BMP from the cardiac mesoderm. Under the influence of these stimuli and processes, physiological liver development and differentiation into hepatocytes ensues [28,29].

By mimicking liver development in vitro, researchers have induced the generation of hepatocyte-like cells (HLCs) from various sources, including stem cells. The key to successful HLCs induction lies in producing cells with a phenotype and function closely resembling primary hepatocytes [31,32]. To achieve this, various induction protocols are being developed. Current protocols typically involve three stages: generation of definitive endoderm, production of hepatic progenitors, and finally, differentiation into functional HLCs. To achieve this process, cell differentiation can be promoted by adding specific cytokines or growth factors at each stage to mimic key in vivo signals [31,32].

Several research groups have investigated the hepatic differentiation process. Promoting definitive endoderm differentiation is the initial crucial step. In this context, Activin A and WNT3 signaling have been identified as key factors. Activin signaling regulates the expression of NANOG, a gene crucial for maintaining stem cell pluripotency. In iPSC models, high levels of Activin A drive definitive endoderm differentiation, while lower levels maintain iPSC pluripotency[33]. Similarly, stimulation of the WNT/β-catenin pathway promotes iPSC differentiation in conjunction with Activin

A [34]. Definitive endodermal consolidation is further induced by BMP-4 and FGF-2/4. These cytokines, pivotal during embryonic development, activate GATA4, promoting liver differentiation while suppressing pancreatic development [34]. During the final stages of liver development, both in embryos and in vitro, HGF, oncostatin M (OSM), and dexamethasone (DEX) are essential for differentiation [35]. The combination of HGF, OSM, and DEX enhances hepatocyte differentiation by upregulating the expression of mature liver-specific genes, such as albumin and CYP450 [6]. The application of this differentiation protocol has been widely studied employing 2D and 3D approaches to obtain HLCs. The simplicity of 2D cultures makes them highly suitable for high-throughput studies, such as drug screening [36]. While 2D systems offer ease of use, hepatic function typically declines within a few days in culture, limiting their application to short-term studies of function and acute toxicity [37]. Furthermore, these models often fail to accurately replicate the complex in vivo environment. Spatially patterning different cell populations within 2D cultures can stabilize hepatic morphology and function for extended periods, enabling chronic toxicity and metabolism studies that are not feasible with other 2D models [38]. However, this approach requires specialized expertise and equipment that may not be readily accessible to all laboratories. On the other hand, 3D culture systems offer significant advantages by recapitulating crucial cell-cell and cell-extracellular matrix interactions that are absent in 2D environments [37,39]. Although 3D cultures often present greater challenges for high-throughput applications, they more accurately reflect the in vivo hepatic microenvironment [40]. Thus, it is crucial to provide appropriate mechanical stimulation and sufficient growth space to further promote cellular differentiation and maturation in 3D culture. One promising approach involves creating a protein-based 3D scaffold that mimics the human liver microenvironment [41]. Consequently, numerous studies have explored strategies to optimize the physical environment for cell growth, including manipulating the matrix, oxygen concentration, and flow conditions, utilizing diverse culture systems.

Hepatocyte-like cells 3D culture-based differentiation

Recent advancements in stem cell research have significantly improved scientists' ability to control cellular differentiation, particularly with MSCs, iPSCs and HLSCs. The development of three-dimensional (3D) cell culture systems has been instrumental in promoting cell differentiation toward specific organ linages, by facilitating cell-to-cell interactions and exchange of soluble molecules, crucial for intercellular signaling [42]. Moreover, the cultivation of hepatocyte-like cells (HLCs) in growth factors-enriched media has proven pivotal role for the *in vitro* hepatic differentiation [43]. By replicating embryonic signals, HLCs differentiation is achieved using fibroblast growth factors 2 (FGF2) and 4 (FGF4), bone morphogenetic protein 4 (BMP4) and HGF. The maturation phase typically involves supplements like oncostatin M (OSM), dexamethasone, and insulin- transferrin-selenium (ITS) premix to encourage full hepatic functionality [35]. Coso et al. have studied the role of two different protocol of differentiation using different factor cocktail comparison. FGF, HGF, EGF, and dexamethasone factors have shown the best result for in vitro differentiation primarily in the presence of 3D microenvironment demonstrated that microenvironment, encouraging growth of MSCs and their differentiation into HLCs essentially in the presence of growth factors [44] .

Early hepatocyte-like induction shows markers such as α-fetoprotein (αFP), Albumin and alpha-1-antitrypsin (A1AT), while full hepatic maturation is indicated by CTP450 enzymes, hepatic transporters, and urea cycle enzymes [6]. For example, Takebe et al. successfully generated vascularized, functional human liver buds using iPSCs, MSCs, and endothelial cells, highlighting the potential of stem cell-based liver models [45]. In a 3D bioreactor system, MSC demonstrated the ability to differentiate into HLCs evaluating markers CK-18, HNF-4*α*, albumin, the hepatic transporters OATP-C and MRP-2 as well as drug-metabolizing enzymes like CYP1A2 and CYP3A4 [46].

In this scenario, HLSCs have shown the ability to differentiate into hepatic-like cells in 3-D model using approaches such as bioartificial liver (BAL) system, scaffolds and Rotary cell culture systems (RCCS). In the BAL environment, HLSCs were able to produce increased levels of albumin, urea,

and HGF and expressed liver-specific markers such as cytochrome P450, suggesting that they had acquired mature hepatocyte characteristics [47]. Likewise, HLSCs differentiated into HLCs in a rat liver acellular scaffold model, expressing CYP450 enzymes and showed urea production [48]. In addition, 3D rotary *in vitro* assay was employed to generate functional hepatocyte-like cells from HLSCs, further validating their potential in liver regenerative models [24].

Aim of the work

The aim of this study is to delve deeper and better characterized the process of hepatic differentiation of human liver stem cells (HLSCs) in the *in vitro* 3D-rotary culture system. The expression of mature hepatic markers, such as CYP 450 cytochromes, urea cycle enzyme, production and release of urea and coagulation factor VIII were followed for over 10 days of culture, together with the evaluation of the hepatic function. Moreover, the expression of the pluripotent stem cell markers was evaluated at different time points during the differentiation process. A multi-assay approach has been employed to first characterized differentiated HLSCs at molecular level, by evaluation expression of different genes and protein typical expressed by stem cells or by mature hepatocytes (Figure 4). To further assess function of our differentiate cells, we aim to quantify the release of urea, the most important waste liver product as an index of the hepatocyte functionality. Likewise, we pursue the establishment of the hepatocyte-like cell function evaluating the uptake of indocyanine green, a green dye used to assess liver donor graft quality and graft metabolic function during transplant procedure. Therefore, our characterization of HLSCs aim to define the hepatocyte-like differentiation capability. Overall, the results obtained could be used for future validation to qualify the capabilities of HLSC as a Good Manufacturing Practice (GMP) drug product to be used in clinical setting.

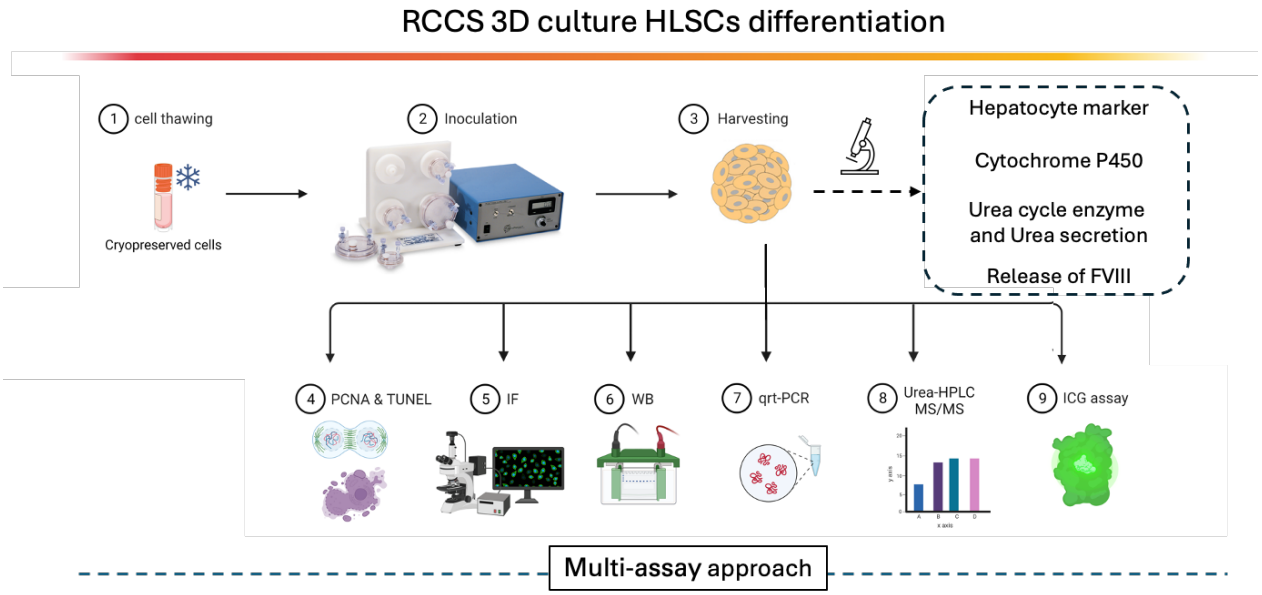

Figure 4: Overview of experimental steps for 3D hepatocyte-like differentiation of HLSC (Created with BioRender.com).

Material and Methods

Cell culture

HLSCs were expanded from a GMP-produced master cell bank (MCB), supplied by Unicyte AG (Switzerland). The MCB was established from 10-15 mm liver fragments from a donor, following the Centro Nazionale Trapianti's standard guidelines [27]. The liver tissue was digested using GMP-grade collagenase (0.6 mg/mL) and neutral protease (0.73 mg/mL) (Nordmark Pharma GmbH, Germany) for 20 minutes at 37°C. The resulting liver cell suspension was washed (400 g, 10 min) and cultured (4×10^4 cells/cm²) in α-MEM (Lonza) with 10% fetal calf serum (Euroclone), 4 ng/mL human recombinant epidermal growth factor (hrEGF, Miltenyi Biotec), 4 ng/mL human recombinant fibroblast growth factor basic (hrFGF2, Miltenyi Biotec), 2 mM L-glutamine (Lonza), and 100 U/mL penicillin/streptomycin (Sigma-Aldrich) in a 5% CO2 humidified incubator at 37°C. After two weeks, HLSCs were seeded at 3×10^3 cells/cm² in T75 flasks in the same medium. Once 80% confluency was reached, cells were expanded for three additional passages and cryopreserved in vials (5×10^6 cells/vial) as MCB stock. The MCB (passage 4) was subcultured for two further passages (to passage 6), creating a working cell bank (WCB). Three WCBs were produced and used for subsequent experiments. All reagents used in the R&D expansion phase adhered to clinical-grade standards and complied with AIFA regulations.

HaCaT cells, kindly provided by Prof. Calautti (MBC, Turin), were cultured in high-glucose DMEM (Thermo Fisher Scientific) supplemented with 2 mM L-glutamine and 10% FCS. Cells were harvested using a 1:1 mixture of 0.05% EDTA and 0.1% trypsin in 1X PBS (without Ca^{2+} and Mg^{2+}). Human hepatocytes (purchased from Lonza) were cultured according to the manufacturer's protocol.

Fluorescence-activated cell sorter (FACS) analysis

The phenotype of HLSCs was characterized through flow cytometry (FACS) analysis using the FACSCelesta™ Cell Analyzer (Becton Dickinson, BD, Biosciences, Franklin Lakes, NJ, USA). The following antibodies were employed: anti-CD44, CD105, CD73, CD90, CD29, CD14, CD34, CD45,

and human albumin. All antibodies are listed in Table 1. Intracellular albumin staining was performed according to the manufacturer's protocol using BD Cytofix/Cytoperm™ (BD Pharmingen). Antibodies conjugated to FITC, PE, or APC were utilized. Corresponding FITC, PE, and APC isotype controls (all from Miltenyi), along with human FITC-isotype controls (LSBio for albumin staining), served as negative controls. Data were analyzed with BD FACSDiva™ Software (BD Biosciences).

In vitro 3D-rotary cell culture system (RCCS) cell differentiation into hepatic lineage

HLSCs were differentiated into hepatocyte-like cells using a modified version of the protocol described by Herrera et al. [24]. Briefly, 5×10^6 cells were resuspended in 10 mL of differentiation media composed of a 60/40 (v/v) mixture of low-glucose DMEM (without phenol red; Euroclone) and MCDB-201 (without phenol red; Cell Technologies, Lugano, Switzerland), supplemented with 2% fetal calf serum (FCS) (Thermo Fisher Scientific), 0.026 g/mL ascorbic acid 3-phosphate, linoleic acid-bovine serum albumin (LA-BSA), insulin-transferrin-selenium (ITS), all from Sigma, as well as 10 ng/mL rhFGF4 and 10 ng/mL rhHGF (both from Miltenyi). The cells were inoculated into rotary vessels (Synthecon, Houston, TX, USA) and rotated at 8 rpm in a clockwise direction. After 1, 4, 7, and 10 days of culture, the cell aggregates and supernatant were separated by centrifugation at 300 g for 5 minutes. Supernatants were collected, aliquoted, and stored at −20°C, while HLSC aggregates were washed with PBS and used for subsequent experiments.

Immunofluorescence staining

Cells were cultured on chamber slides (Nalgene Nunc International, Rochester, NY) and fixed with 4% paraformaldehyde, followed by permeabilization using a Hepes-Triton X-100 buffer (Sigma-Aldrich). HLSC aggregates retrieved from RCCS at various time points (days 1, 4, 7, and 10) were directly embedded in OCT (Bio-Optica, Milan, Italy) and sectioned into 10 µm slices. The sections were fixed with precooled ethanol/acetic acid (2:1) at room temperature for 5 minutes. After blocking in PBS with 1% BSA (Sigma-Aldrich) for 1 hour, cells and slices were stained with primary and secondary antibodies. Markers for stem cells (anti-OCT3/4, anti-Nanog, anti-Sox2, anti-KLF4), early

hepatic differentiation (anti-HNF4a, anti-αFP), and proliferation (anti-PCNA) were analyzed. Mature hepatic markers (anti-human albumin, anti-OATP1B1, anti-cytokeratin 18, anti-cytokeratin 8), cytochrome enzymes (anti-CYP1A1, anti-CYP3A4, anti-CYP7A1), urea cycle enzymes (anti-OTC, anti-ASS1, anti-CPS1, anti-ARG1, anti-ASL), and coagulation factors (anti-FVIII) were further employed for cell and aggregate characterization. Detection was carried out using secondary antibodies such as Alexa Fluor 488 goat anti-mouse IgG, anti-rat, donkey anti-goat, and Alexa Fluor 594 chicken anti-mouse IgG. Controls included omission of primary antibodies or replacement with nonimmune rabbit, rat, or mouse IgG. All antibodies are listed in Table 1. SlowFade Gold antifade reagent (Thermo Fisher Scientific, Eugene, OR, USA) was used for nuclear staining alongside fluorescence labeling. Human hepatocytes served as positive controls for urea cycle enzyme expression. Confocal microscopy was performed using the Leica SP8 Confocal Microscope (Wetzlar, Germany), with images analyzed using ImageJ software (https://imagej.nih.gov/).

Terminal dUTP nick end-labeling (TUNEL) assay

Apoptosis was quantified using the TUNEL assay (Merck Millipore, Darmstadt, Germany) following the manufacturer's protocol. Briefly, HLSCs were seeded, and HLSC aggregates were sectioned and fixed as previously described. Samples were treated with terminal deoxynucleotidyl transferase enzyme and incubated in a humidified chamber at 37°C for 1 hour. Subsequently, the sections were incubated with fluorescein isothiocyanate (FITC)-conjugated anti-digoxigenin for 30 minutes at room temperature. SlowFade Gold antifade reagent (Thermo Fisher Scientific, Eugene, OR, USA) was used for mounting and nuclear staining. TUNEL-positive nuclei and total nuclei were analyzed using a Leica SP8 Confocal Microscope (Wetzlar, Germany) with Leica Navigator software. Nuclei counting was performed with ImageJ software (https://imagej.nih.gov/).

Periodic acid Schiff staining

HLSC aggregates were collected. The samples were formalin-fixed and paraffin-embedded, then cut for the histological analysis. Deparaffinized, hydrated rinsed process were used to prepare the section

for the staining. The sections were then incubated with 0.5% periodic acid solution for 5 min, stained with Schiff' reagent for 15 min, and counterstaining with hematoxylin solution for 2 min. All steps were performed at room temperature.

Western blot

Cells and cells aggregates were carefully collected, washed with 1X PBS and snap-frozen before the use. Therefore, samples were lysed using RIPA Buffer (RIPA + PMSF + protease inhibitors, all of them purchased by Sigma-Aldrich) on ice for 15 min to induce cell lysis and then centrifuged at 12,000 g for 15 min at 4°C. For protein quantification, the PierceTM BCA Protein Assay Kit (Thermo Fisher Scientific) was utilized, according to the manufacturer's protocol, and the absorbance was read at 562 nm on an iMark Microplate reader (Bio-Rad, Hercules, CA, United States). Briefly, 4–20% gradient mini-PROTEAN TGX precast electrophoresis gels (Bio-Rad) were used to separate proteins, before transferring them onto 0.2µm nitrocellulose membranes. After saturation in 5% milk 0.1% Tween-20 (PBS-T) blocking solution for 2h at room temperature. Then, membranes were incubated with specific primary antibody at 4°C over-night. For the detection of the investigated protein, membranes were incubated with HRP-conjugated secondary antibody (Thermo Fisher Scientific), with a dilution of 1:3000 in PBS-T. After incubation with the Amersham TM enhanced chemiluminescence substrate (Cytiva, Little Chalfont, United Kingdom), the chemiluminescent signal was detected using the Chemidoc system (Bio-Rad).

GAPDH and vinculin were employed to normalize the data. Results were presented as density units and analyzed with ImagLab software (Bio-Rad). For the analysis of FVIII release into the supernatant, the samples were collected and immediately frozen (Antibody listed in table 1). At first, the samples were processed with 50 kDa filter spin columns (Millipore, Burlington, MA, United States) and then the flowthrough was concentrated hundred-fold using 10kD filter spin columns (Abcam) according to the manufacturer's instructions.

Antibody	**Catalogue number**
CD44	Miltenyi, 130-113-342
CD105	Miltenyi, 130-112-321
CD73	BD pharmingen, 560847
CD90	Miltenyi, 130-117-684
CD29	Miltenyi, 130-101-256
CD14	Miltenyi, 130-110-577
CD34	BD pharmingen, 555821
CD45	BD pharmingen, 555482
human Albumin-FITC	LSBIO, LS–C68850
human Albumin-FITC- isotype	LSBIO, LS-C149360
PE -isotype	Miltenyi, 130-113-200
FITC-isotype	Miltenyi, 130-113-199
APC-isotype	Miltenyi, 130-113-196
PCNA	Santa Cruz, sc-56
OCT3/4	R&D, MAB1759
NANOG	R&D, AF1997
SOX2	R&D, MAB2018
KLF4	R&D, AF3640
HNF4a	Abcam, 92378
ALBUMIN	R&D, MAB1455
Cytokeratin 18	Abcam, ab52948
OATP1B1/OATP2	Novusbio, NB100-74481
CYP1A1	Santa Cruz, sc-25304
CYP3A4	Santa Cruz, sc-53850
CYP7A1	Santa Cruz, sc-518007
OTC	Abcam, Ab262864
ASS1	Abcam, Ab124465 Abcam, Ab170952
CPS1	Abcam, Ab37168 Abcam, Ab45956
ARG1	Abcam, Ab239731
ASL	Abcam, Ab201025

	Abcam, ab97370
FVIII	Abcam, ab236284 Abcam, ab171825
CK8	Abcam, ab59400
alpha Fetoprotein	R&D, MAB1368
GAPDH	Abcam, Ab37168
Vinculin	Self-made, kindly provided by Prof. Turco (MBC, Torino)
mouse IgG2a (negative control for OTC).	Abcam, ab18415
rabbit IgG polyclonal (negative control for ASS1)	Abcam, ab17273
rabbit IgG polyclonal (negative control for CPS1 and AGL)	Abcam, ab171870
mouse IgG2b (negative control for ARG)	Abcam, ab18469
Alexa Fluor 488 goat anti-rabbit IgG	Invitrogen, A11008
Alexa Fluor 546 goat anti-mouse IgG	Invitrogen, A11003
Alexa Fluor 594 chicken anti-goat IgG	Invitrogen, A21468
Alexa Fluor 488 goat anti-rat IgG	Invitrogen, A11006
Alexa Fluor 488 donkey anti-goat IgG	Invitrogen, A11055

Gene expression analysis by real time PCR

Gene expression analysis was performed using real-time PCR. Total RNA was extracted from HLSCs (passages 6/7) and RCCS aggregates (day 1 and day 4) with the miRNeasy Micro Kit (Qiagen, Hilden, Germany) following the manufacturer's instructions. RNA concentrations were measured using a Nanodrop ND-2000 (Thermo Fisher Scientific), and the eluted RNA was stored at −80°C for later use. Liver-related genes were screened using a custom RT² Profiler PCR Array was designed via the Qiagen Gene Globe platform (Table 2). For the analysis, 1 µg of total RNA was reverse transcribed using the RT² First Strand Kit (Qiagen) per the manufacturer's guidelines. The resulting cDNA, along with RT² SYBR Green ROX™ qPCR Master mix, was applied to custom PCR array cards and run on the Step OnePlus real-time PCR system (Applied Biosystems, Foster City, CA). Five endogenous controls (ACTB, HPRT1, GUSB, GAPDH, B2M) were utilized, along with retro transcription,

genomic contamination, and reproducibility controls. Data analysis was conducted using the Gene Globe software, with results expressed as fold changes (2−ΔΔCt) or via the Expression Suite software (Applied Biosystems). ΔΔCt represents the normalized gene expression (2−ΔCt) in the test sample divided by the control sample. Biological replicates (n = 5) were run in duplicate.

For specific gene expression analysis, quantitative real-time PCR (qRT-PCR) was conducted. First-strand cDNA was synthesized from 200 ng of total RNA using the High-Capacity cDNA Reverse Transcription Kit (Applied Biosystems). qRT-PCR was performed using the StepOnePlus machine in a 20 μL reaction containing 5–10 ng of cDNA, gene-specific primers (Eurofins Scientific, Brussels, Belgium), and Power SYBR Green PCR Master Mix (Applied Biosystems). TBP served as the endogenous control. Fold change expression relative to the control was calculated using the ΔΔCt method. The primers sequence used are listed in Table 3.

Refseq	Symbol	Description	Name
NM_000463	UGT1A1	UDP glucuronosyltransferase 1 family, polypeptide A1	BILIQTL1/GNT1/HUG-BR1/UDPGT/UDPGT 1-1/UGT1/UGT1A
NM_019093	UGT1A3	UDP glucuronosyltransferase 1 family, polypeptide A3	UDPGT/UDPGT 1-3/UGT-1C/UGT1-03/UGT1.3/UGT1A3S/UGT1C
NM_007120	UGT1A4	UDP glucuronosyltransferase 1 family, polypeptide A4	HUG-BR2/UDPGT/UDPGT 1-4/UGT-1D/UGT1-04/UGT1.4/UGT1A4S/UGT1D
NM_002701	POUF5F1	POU class 5 homeobox 1	OCT3/OCT4/OTF-3/OTF3/OTF4/Oct-3/Oct-4
NM_022454	SOX17	SRY (sex determining region Y)-box 17	VUR3
NM_021784	FOXA2	Forkhead box A2	HNF3B/TCF3B
NM_002273	KRT8	Keratin 8	CARD2/CK-8/CK8/CYK8/K2C8/K8/KO
NM_000224	KRT18	Keratin 18	CK-18/CYK18/K18
NM_002276	KRT19	Keratin 19	CK19/K19/K1CS
NM_004364	CEBPA	CCAAT/enhancer binding protein (C/EBP), alpha	C/EBP-alpha/CEBP
NM_005194	CEBPB	CCAAT/enhancer binding protein (C/EBP), beta	C/EBP-beta/IL6DBP/NF-IL6/TCF5

NM_000545	HNF1A	HNF1 homeobox A	HNF-1A/HNF1/IDDM20/LFB1/MODY3/TCF-1/TCF1
NM_000458	HNF1B	HNF1 homeobox B	FJHN/HNF-1-beta/HNF-1B/HNF1beta/HNF2/HPC11/LF-B3/LFB3/MODY5/TCF-2/TCF2/VHNF1
NM_178849	HNF4A	Hepatocyte nuclear factor 4, alpha	FRTS4/HNF4/HNF4a7/HNF4a8/HNF4a9/HNF4alpha/MODY/MODY1/NR2A1/NR2A21/TCF/TCF14
NM_004498	ONECUT	One cut homeobox 1	HNF-6/HNF6/HNF6A
NM_000295	SERPINA1	Serpin peptidase inhibitor, clade A (alpha-1 antiproteinase, antitrypsin), member 1	A1A/A1AT/AAT/PI/PI1/PRO2275/alpha 1AT
NM_000477	ALB	Albumin	ANALBA/FDAH/PRO0883/PRO0903/PRO1341
NM_001134	AFP	Alpha-fetoprotein	AFPD/FETA/HPAFP
NM_000277	PAH	Phenylalanine hydroxylase	PH/PKU/PKU1
NM_000499	CYP1A1	Cytochrome P450, family 1, subfamily A, polypeptide 1	AHH/AHRR/CP11/CYP1/P1-450/P450-C/P450DX
NM_000761	CYP1A2	Cytochrome P450, family 1, subfamily A, polypeptide 2	CP12/P3-450/P450(PA)
NM_000104	CYP1B1	Cytochrome P450, family 1, subfamily B, polypeptide 1	CP1B/CYPIB1/GLC3A/P4501B1
NM_000767	CYP2B6	Cytochrome P450, family 2, subfamily B, polypeptide 6	CPB6/CYP2B/CYP2B7/CYP2B7P/CYPIIB6/EFVM/IIB1/P450
NM_000771	CYP2C9	Cytochrome P450, family 2, subfamily C, polypeptide 9	CPC9/CYP2C/CYP2C10/CYPIIC9/P450IIC9
NM_017460	CYP3A4	Cytochrome P450, family 3, subfamily A, polypeptide 4	CP33/CP34/CYP3A/CYP3A3/CYPIIIA3/CYPIIIA4/HLP/NF-25/P450C3/P450PCN1
NM_000765	CYP3A7	Cytochrome P450, family 3, subfamily A, polypeptide 7	CP37/CYPIIIA7/P-450(HFL33)/P-450111A7/P450-HFLA
NM_000780	CYP7A1	Cytochrome P450, family 7, subfamily A, polypeptide 1	CP7A/CYP7/CYPVII
NM_001875	CPS1	Carbamoyl-phosphate synthetase 1, mitochondrial	CPSASE1/PHN
NM_000050	ASS1	Argininosuccinate synthase 1	ASS/CTLN1
NM_000531	OTC	Ornithine carbamoyltransferase	OCTD
NM_000045	ARG1	Arginase, liver	-
NM_000048	ASL	Argininosuccinate lyase	ASAL
NM_001101	ACTB	Actin, beta	BRWS1/PS1TP5BP1
NM_004048	B2M	Beta-2-microglobulin	-
NM_000194	HPRT1	Hypoxanthine phosphoribosyltransferase 1	HGPRT/HPRT

NM_002046	GAPDH	Glyceraldehyde-3-phosphate dehydrogenase	G3PD/GAPD/HEL-S-162eP
NM_000181	GUSB	Glucuronidase, beta	BG/MPS7
SA_00104	RTC	Reverse Transcription Control	RTC
	PPC	Inter Plate Reproducibility Control	PPC
SA_00105	HGDC	Human Genomic DNA Contamination	HIGX1A

Table 2: List of genes analyzed in PCR array panel

Gene name	Forward primer (5'-3')	Reverse primer (5'-3')
h-SLCO1B1	ACTGATTCTCGATGGGTTGGAG	TGTTTCCAGCACATGCAAAGAC
h-TBP	TGTGCACAGGAGCCAAGAGT	ATTTTCTTGCTGCCAGTCTGG
h-FVIII	CTGTGGACGCAAGATTTCCTC	AGGATGGGAAGCCATGTTCTT

Table 3: Specific Primers pairs used

Urea quantification by HPLC-MS/MS and QuantiChrom™ Urea Assay analysis

Urea production was measured by liquid chromatography hyphenated with tandem mass spectrometry (LC-MS/MS). Urea chromatographic separations were performed on a Nexera HPLC (Shimadzu, Kyoto, Japan) coupled to a Qtrap mass spectrometer (Sciex 5500, Framingham, MA, United States) equipped with an ESI Turbo Ion Spray source. Supernatant samples from RCCS experiments were analyzed using a hydrophilic interaction liquid chromatography (HILIC) column (Phenomenex Luna HILIC 150 × 2.1 mm, 3 μm particle size, Phenomenex, Torrance, CA, United States) at a flow rate of 200 μL/min. A gradient mobile phase composition was used: 95/5 to 20/80 solvent A/solvent B. Solvent A was acetonitrile and solvent B was 5 mM aqueous ammonium acetate with 2% of acetonitrile. The injection volume was 20 μL. The tuning parameters used for the ESI source were: source voltage 4.5 kV (positive ion mode), source temperature 300°C, and curtain gas nitrogen. Analyses were performed using selected reaction monitoring MS/MS acquisition, with a precursor ion 61 m/z, a product ion 44 m/z, and a collision energy 20 V. The lower limit of quantification (LLOQ) was 50 ng/mL (supernatant samples were tenfold diluted with acetonitrile before injection). Data were expressed as parts per million (ppm, μg/mL). An external urea standard curve (Sigma-Aldrich) was used to quantify the concentration of the samples.

To further quantify urea levels, we employed the QuantiChrom™ Urea Assay Kit-DIUR 100 (BioAssay Systems, CA, United States). This kit utilizes an improved Jung method that directly measures urea in supernatant without the need of prior treatment. The method employs a chromogenic reagent that forms a specific-colored complex with urea. The absorbance of the resulting color, measured at 520 nm, was directly proportional to the urea concentration in the sample.

Statistical analysis

Raw data were analyzed using GraphPad Prism 6.0 software (GraphPad Software, San Diego, CA, United States). Results are expressed as the mean ± standard deviation of 3-5 independent biological replicates. Statistical analyses were performed using one-way analysis of variance (ANOVA) followed by Newman–Keuls comparisons test or Student's t-test, as appropriate. A p-value of <0.05 was considered statistically significant.

Results

HLSC characterization cultured in 2D condition

HLSCs were isolated from a liver biopsy under GMP conditions [27], then expanded and cryopreserved in a WCB at passage 6. Throughout expansion, the HLSC-WCB retained a spindle-shaped morphology without any signs of overgrowth or cellular distress, reaching over 80% confluence (Figure 5A). The proliferative capacity and reproducibility of the cell bank were assessed by measuring the cumulative population doubling (CPD) of the cells following 2D expansion. As illustrated in Figure 5B, no statistically significant differences in CPD were observed up to passage 6. To confirm the identity of the HLSCs, a panel of surface markers were analyzed by fluorescence-activated cell sorter (FACS) and immunofluorescence analysis.

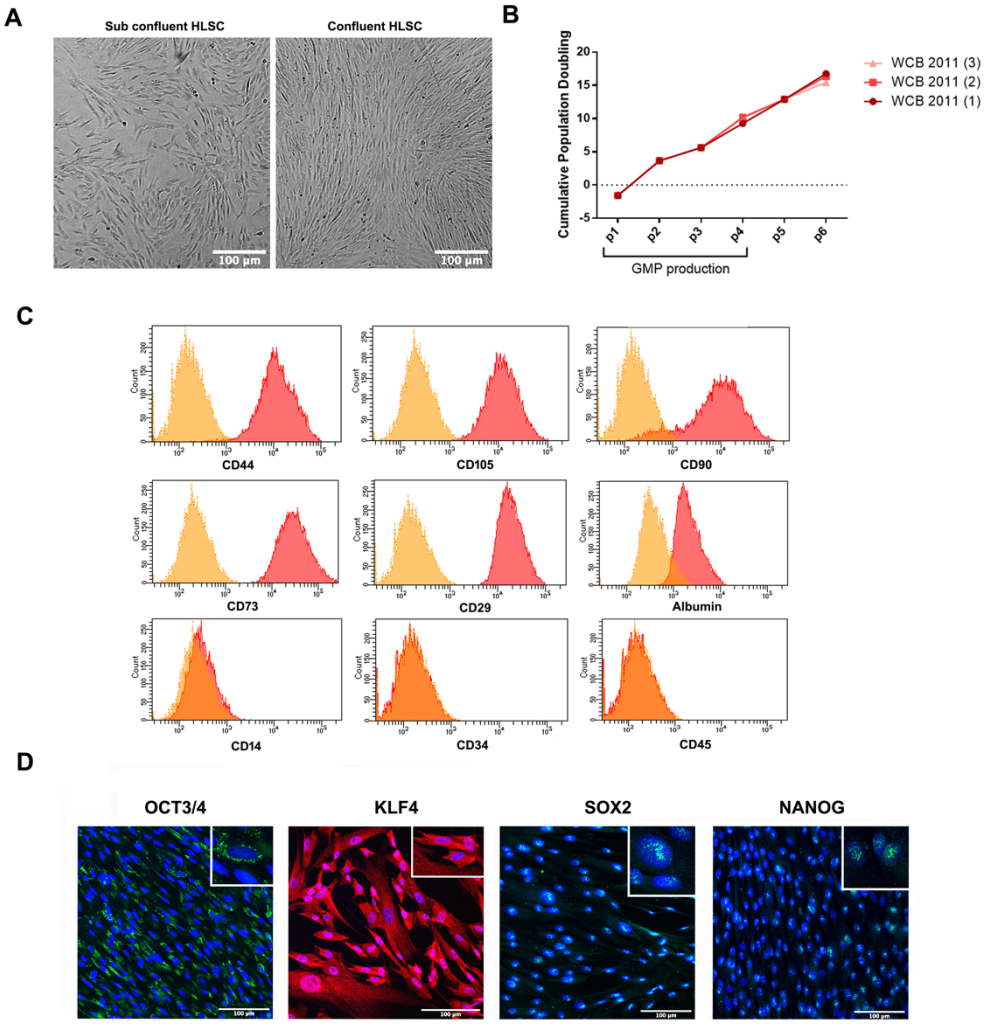

Figure 5: HLSC characterization. **(A)** Representative micrograph showing HLSC morphology. **(B)** Cumulative population doubling (CPD) of three different cell batches of HLSCs from passage 0 to 6. **(C)** Representative FACS analysis for the positive surface markers CD44, CD105, CD73, CD90, CD29 and albumin and the negative markers CD34, CD45, and CD14. **(D)** Representative immunofluorescence micrograph of stem cell markers Nanog, SOX2, KLF4, OCT3/4 in undifferentiated HLSCs. Scale bar, 100μm; magnification × 40, insert pictures. Nuclei are stained in blue with DAPI.

The analysis showed that HLSCs expressed high levels (≥90%) of CD29, CD73, CD90, CD105, and CD44, while lacking expression of the immune cell marker CD14, the hematopoietic cell marker CD45, and the hematopoietic stem cell marker CD34. Additionally, albumin expression was confirmed [24] (Figure 5C). Consistent with previous immunofluorescence analysis, HLSC expressed OCT3/4, SOX2 and Nanog [24] and we further observed KLF4 expression in these cells (Figure 5D). Nanog and SOX2 were localized in the nucleus of HLSCs, KLF4 was found in the cytoplasm, and OCT3/4 was localized in the perinuclear region (Figure 5D).

Characterization of HLSC aggregates in rotary cell culture system

HLSCs were differentiated in proper conditions until the end of the assay as reported in Figure 6A. Cell aggregates and HLSCs were analyzed for proliferating cell nuclear antigen (PCNA) and TUNEL. In addition, Periodic acid–Schiff (PAS) staining was performed after 4, 7 and 10 days of HLSC culture in RCCS (Figure 6). PCNA staining revealed no proliferation of HLSCs during differentiation compared to undifferentiated HLSCs (Figure 6B). Apoptosis measured by TUNEL staining, was evident in HLSC aggregates, with a gradual increase from 11.9% ± 3.2% on day 4%–77.1% ± 6.1% on day 10 (Figures 6C, D). In contrast, on undifferentiated HLSC, no apoptotic cells were observed (Figure 6C). PAS staining, a marker of glycogen synthesis and hepatocyte function, showed PAS-positive areas on the surface of the aggregates, suggesting the presence of glycogen-producing cells on the outer part of the structure (Figure 6E). Based on the TUNEL and PAS staining results, we

decided to focus up to day 4 as the optimal time point for further analysis. For comparison, some experiments were also conducted on day 7.

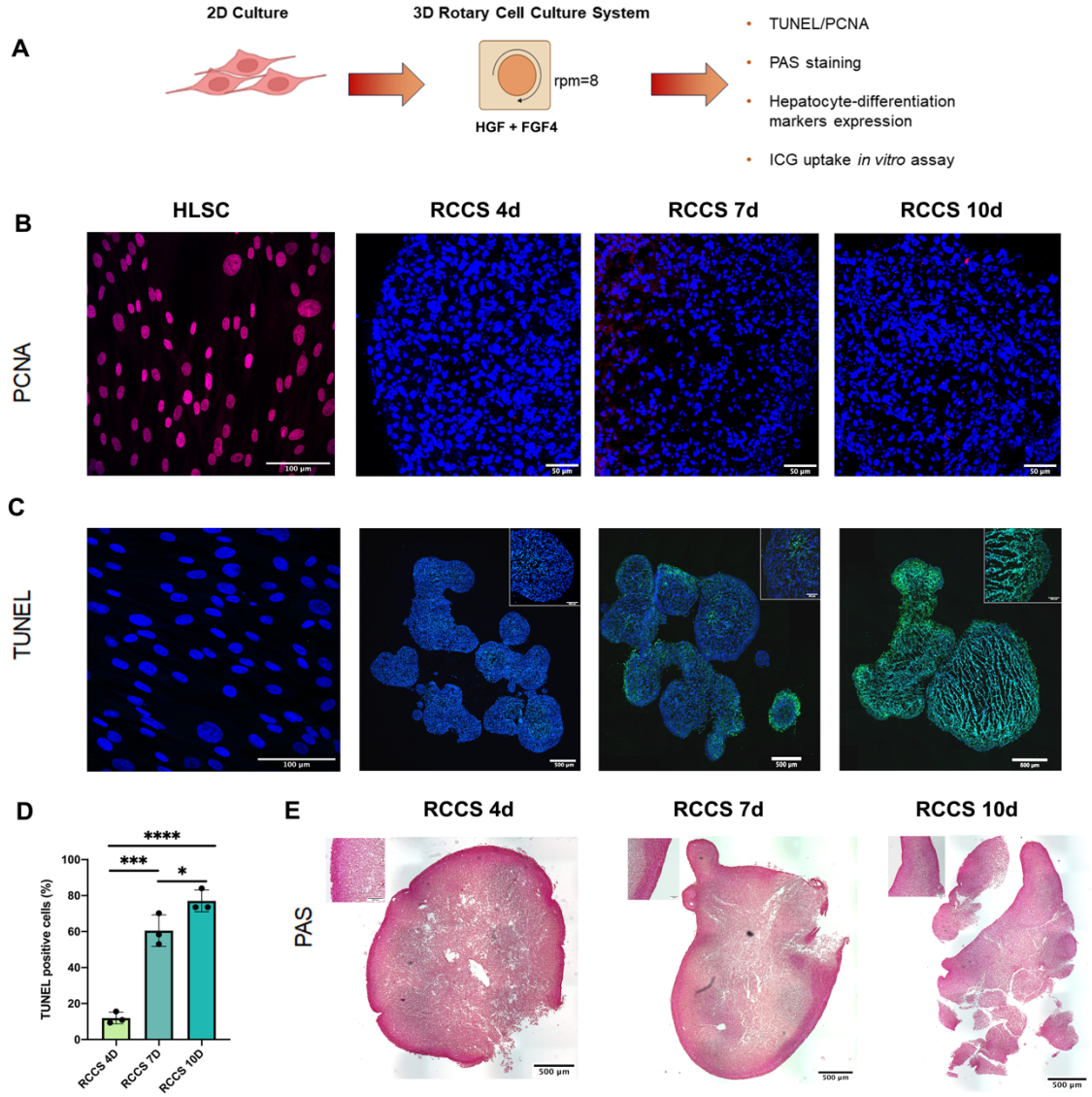

Figure 6: *In vitro* differentiation of HLSCs into hepatocyte-like cells in RCCS. (A) Experimental layout. Created with Biorender.com. (B) Representative PCNA staining of undifferentiated HLSC and differentiation HLSCs in RCCS after 4-, 7- and 10-days. Scale bar, 50, 100 µm. × 40 magnification. HLSCs were used as a positive control. Nuclei (blue) were stained with DAPI. (C) Apoptotic cell death was detected by TUNEL (green), and the nucleus (blue) was stained with DAPI. Scale bar, 500 µm; insert pictures, 100 µm. × 20 magnification. HLSCs were used as an internal control. (D) Quantification of TUNEL-positive cells in all the experimental groups. Values represent the mean ± SD from three independent experiments (black dots represent the experimental replicates). ***$p < 0.0001$ RCCS 4d vs. RCCS 7d, *$p < 0.05$ RCCS 7d vs. RCCS 10d, ****$p < 0.001$ RCCS 4d vs. RCCS 10d. (E) PAS staining of RCCS aggregates analyzed at day 4, 7, and 10 post-differentiation. Scale bar, 500µm, insert pictures, 100 µm, ×20 magnification.

Differential gene expression analysis by PCR array

To evaluate the maturation state of HLSCs into hepatocyte-like cells, gene expression profiles of undifferentiated and RCCS-differentiated HLSCs were compared, using PCR array analysis (Figure 7). Hepatocytes were used as positive control of fully differentiated cells. Our results identified distinct gene expression profiles between undifferentiated and differentiated HLSCs. Clustering analysis revealed significant changes in hepatic gene expression across all groups examined (Figure 7). Following exposure to RCCS, as shown by Volcano plot analysis (Figures 7 B, C) 13 out of 32 genes showed significant modulation (9 upregulated and 4 downregulated) in HLSCs after day 1, while 19 out of 32 genes were significantly modulated (15 upregulated and 4 downregulated) after 4 days. Most of these differentially expressed genes encode hepatic signaling molecules crucial for liver development and are typically expressed in mature hepatocytes (Figure 7).

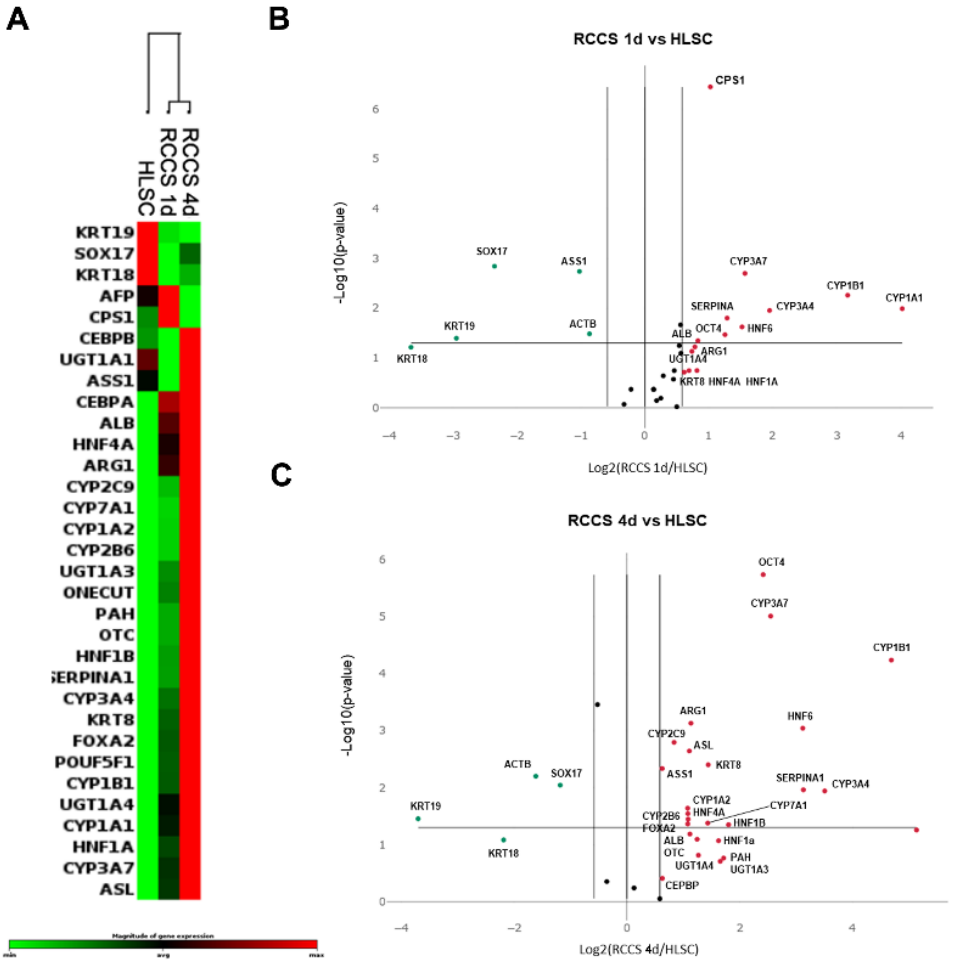

Figure 7: PCR array Gene expression analysis. (A) Heatmap of gene expression of the three biological groups analyzed (n = 5: number of independent experiments x group); RCCS 1d, and RCCS 4d cluster together, and undifferentiated HLSCs are separated from RCCS samples. (B) Volcano plot comparing gene expression of HLSCs vs. RCCS day 1 and (C) vs. RCCS day 4. Red dots represent upregulated genes and green dots represent downregulated genes. All dots above the p-value line are statistically significant with respect to control.

The list of upregulated mature hepatocyte genes in RCCS-differentiated HLSCs included *KRT8*, *UGT1A3*, *UGT1A4*, *POUF5F1*, *FOXA2*, *CEBPB*, *HNF1A*, *HNF4A*, *HNF6*, *ALB*, *PAH*, *CYP1A1*, *CYP1A2*, *CYP1B1*, *CYP2B6*, *CYP3A4*, *CYP3A7*, *CYP7A1*, *SERPINA1*, *CPS1*, *OTC*, *ARG1*, and *ASL* (Figure 7). Thus, the expression of both genes and proteins involved in hepatic differentiation were investigated in RCCS-cultured HLSCs compared to undifferentiated HLSCs.

Immunofluorescence and RT-PCR analysis of hepatocyte-like differentiated HLSCs

To assess the efficiency of our hepatic differentiation system, we characterized HLSC aggregates by evaluating the expression of specific liver markers (Figure 8). As previously demonstrated [24], albumin was highly expressed in undifferentiated HLSCs (Figure 8A). During differentiation, albumin expression remained stable in RCCSs (Figure 8A), exhibiting a transition from cytoplasmic localization to granular localization after 1 day. On the other hand, albumin mRNA expression exhibited a twofold increase during differentiation in RCCS (Figure 8B). CK8, a marker of mature hepatocytes, showed low expression in undifferentiated HLSCs but significantly increased during differentiation in RCCS, both at the protein and gene levels (Figures 8). HNF4, a transcription factor essential for liver development, was highly expressed in undifferentiated HLSCs and remained consistent throughout differentiation, as depicted in Figure 7A. This finding was further supported by the absence of significant changes in mRNA expression levels (Figure 8B). αFP, a marker of immature hepatoblasts [49], was markedly reduced in differentiated HLSCs compared to their undifferentiated counterparts at both the protein and gene levels (Figures 8A, B). CYP450 enzymes, critical for drug metabolism and a hallmark of mature hepatocytes, also displayed an increase during differentiation. Specific CYP isoforms, including CYP1a1, CYP3a4, and CYP7a1, were expressed at low levels in HLSCs and increase during differentiation (Figures 8A, B). These findings demonstrate

that RCCS is able to promotes hepatic differentiation in HLSCs, resulting in the expression of key liver markers and functional enzymes.

Human hepatocytes were used as positive controls for fully differentiated cells, as confirmed by their expression of albumin, CYP1A1, CYP3A4, CYP7A1, CK8. In contrast, HNF4 and αFP showed lower expression levels in human hepatocytes (Figure 8A).

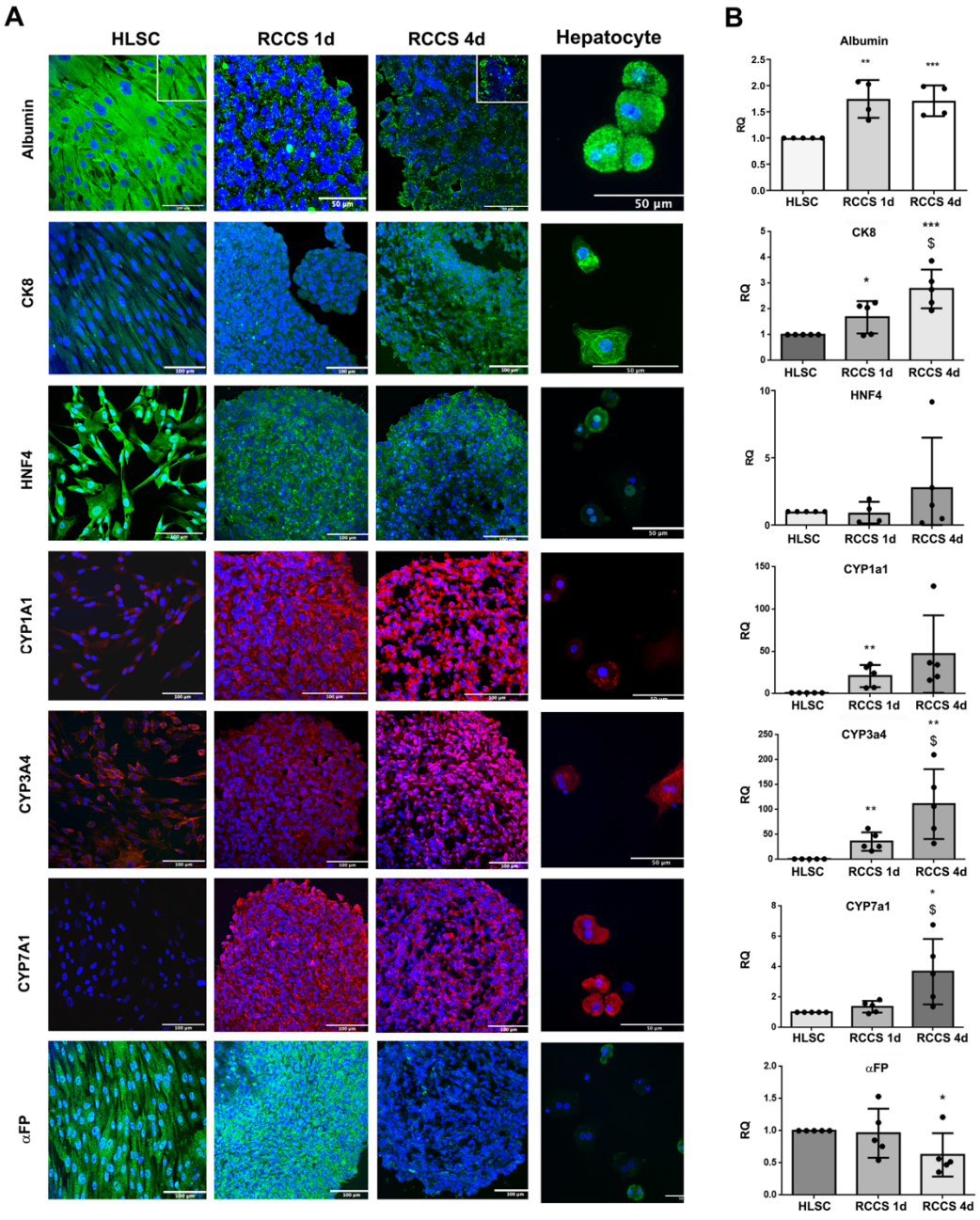

Figure 8: Hepatic markers. (A) Representative immunofluorescence micrographs of Albumin, CK8, HNF4, cytochrome P450 isoform CYP1a1, CYP3a4, CYP7a1 and αFP, in HLSCs and HLSC aggregates after differentiation in RCCS. Human hepatocyte cells were used as positive control. Scale bar, 50 and 100 µm; magnification ×40, insert pictures (albumin staining). Nuclei are stained in blue with DAPI. (B) Real-time PCR array data analysis of hepatic markers of undifferentiated and differentiated HLSCs. Results are expressed as Relative Quantification (RQ), data were normalized

using TBP and undifferentiated HLSCs were used as experimental control. The results are presented as mean values of five independent experiments ±SD *p< 0.05, **p< 0.01, ***p< 0.001 RCCS 1d and 4d vs. HLSC, $^{\$}$p< 0.05 RCCS 4d vs. RCCS 1d.

Expression of coagulation factor

In order to assess the expression of coagulation factor, immunofluorescence staining FVIII, was performed in undifferentiated HLSCs and differentiated counterpart (Figure 9). HLSCs showed strong positive staining for FVIII (Figure 9A). Interestingly, FVIII expression significantly decreased at both the protein and gene levels after 4 days of differentiation in HLSCs (Figures 9A, B). The mRNA expression of FVIII in human hepatocytes was approximately tenfold higher than in differentiated HLSCs (Figure 9B).

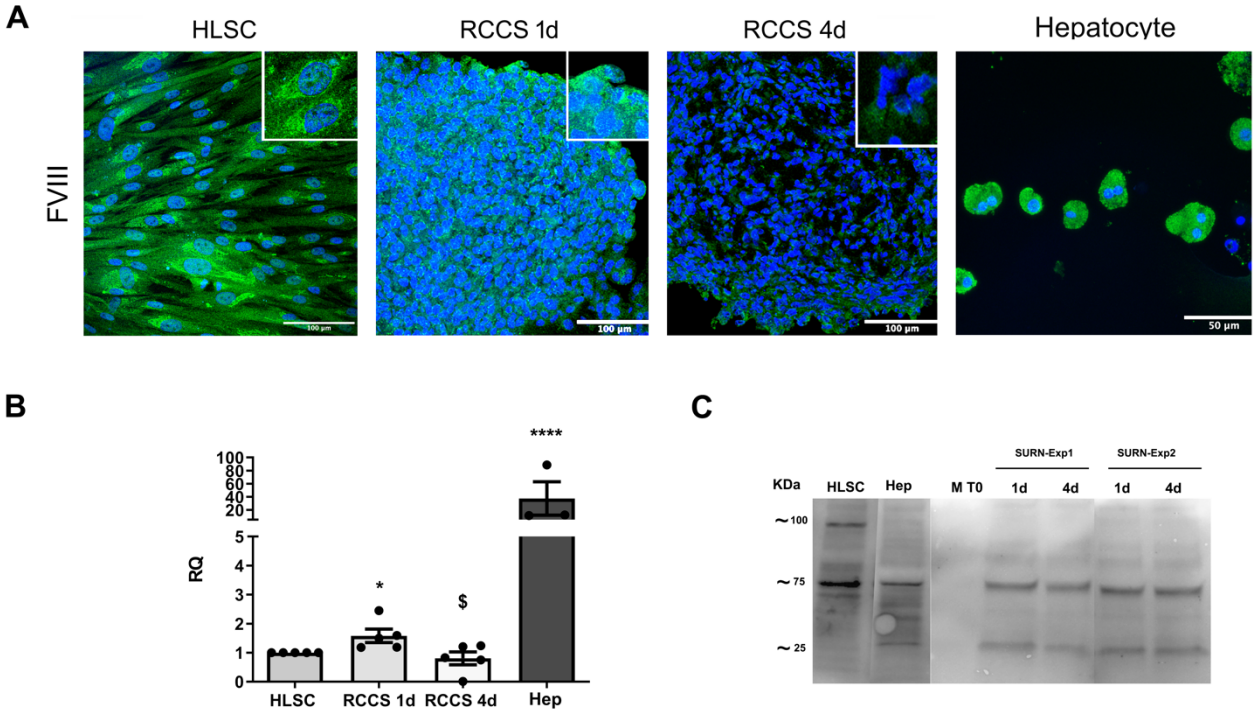

Figure 9: Expression of Coagulation Factor VIII. **(A)** Representative immunofluorescence micrographs of coagulation factor FVIII in HLSCs and differentiated HLSC in RCCS after 1 and 4 days. Human hepatocyte cells were used as positive control. Scale bar, 100 µm. Magnification × 40, insert pictures. Nuclei are stained in blue with DAPI. **(B)** Real-time PCR analysis of FVIII in HLSC, HLSC differentiated after 1 and 4 days, and human hepatocyte (Hep). Results were normalized using TBP and undifferentiated HLSCs were used as experimental control. Real time data are expressed as Relative Quantification (RQ). The results are presented as mean values of five independent experiments ±SD. *p< 0.05 RCCS 4d vs. HLSC; $^{\$}$$p$< 0.05 RCCS 4d vs. RCCS 1d, ****p< 0.0001 Hep vs. HLSC. **(C)** Representative Western Blot of FVIII in HLSCs, human hepatocyte (Hep) and HLSC supernatants after differentiation. M T0: differentiation media at t0 (without HLSCs), 1d and 4d: are supernatants collected after 1 and 4 days of HLSC differentiation in RCCS from two different experiments (SURN-Exp1 and SURN-Exp2).

To explore whether this reduction was linked to FVIII secretion, as observed in hepatocytes, we quantified FVIII levels in the culture supernatant. The reduction in FVIII expression in the 3D aggregates corresponded with an increased release of FVIII into the supernatant (Figure 9C). These results indicate that HLSCs are capable of producing coagulation factor, with FVIII secretion increasing during differentiation.

Induction of urea metabolism in HLSCs differentiate hepatocyte-like cells.

The urea cycle, the primary pathway for removing waste nitrogen generated from protein turnover, is mainly localized in the liver [50]. This energy-dependent process, which begins in the mitochondria and concludes in the cytoplasm, is essential for maintaining nitrogen homeostasis and preventing ammonia toxicity [50]. Impairments in the urea cycle can result in the accumulation of toxic ammonia (NH_4^+), leading to clinical symptoms such as lethargy, slurred speech, cerebral edema, and asterixis [51,52].To evaluate the functionality of the urea cycle in differentiated HLSCs, we quantified urea secretion in RCCS supernatants using mass spectrometry. Compared to the control medium, urea secretion was significantly elevated by day 1 and remained stable through day 7 (Figure 10). These results indicate that differentiated HLSCs are capable of synthesizing and secreting urea, with the majority of production occurring in the early stages of differentiation.

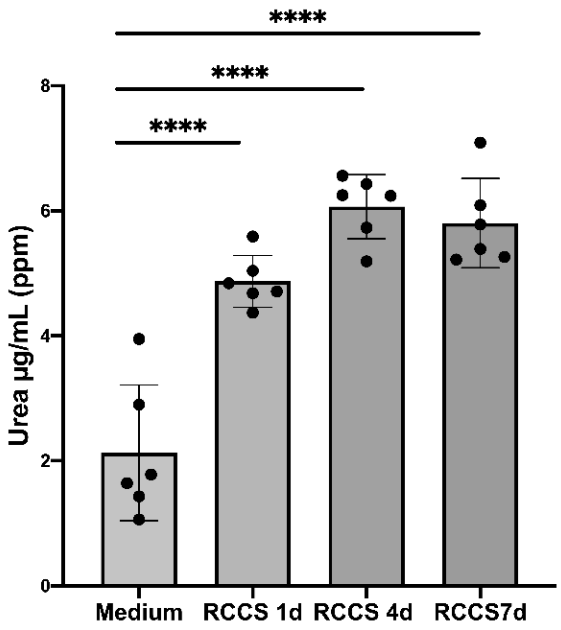

Figure 10: Increase in hepatocyte function of HLSCs under differentiation culture condition. Urea secretion was quantified by HPLC MS/MS analysis. Results were expressed as ppm (part per million) (µg/mL) of urea. The results are presented as mean values of six independent experiments ±SD. ****$p<$ 0.0001 RCCS 1,4,7d vs Medium (without HLSCs).

We further evaluated the expression of urea cycle enzymes in undifferentiated and differentiated HLSCs (Figure 11). Undifferentiated HLSCs exhibited low expression levels of Carbamoyl-Phosphate Synthetase 1 (CPS1), Arginino-succinate lyase (ASL), and Arginase 1 (ARG1), while Arginino-succinate Synthase 1 (ASS1) expression was high, consistent with previous findings [53]. Of note, Ornithine Transcarbamylase (OTC) was not detected in undifferentiated HLSCs (Figure 10A). Immunofluorescence and Western blot analyses showed that the protein levels of all five urea cycle enzymes increased one day after differentiation (Figures 11A, B). However, the relative protein expression between undifferentiated HLSCs and HLSC aggregates cultured in the RCCS remained largely unchanged, except for CPS1, which exhibited a significant increase at both day 4 and day 7 of RCCS culture (Figure 11B).

PCR analysis further confirmed the upregulation of all five urea cycle genes after 1 and 4 days, apart from ASS1, which showed downregulation (Figure 11C). Overall, these findings suggest that RCCS effectively stimulates the expression of urea cycle enzymes (Figure 11D) and enhances urea synthesis in differentiated HLSCs, implying a potential role for these cells in ammonia detoxification and nitrogen balance maintenance. Human hepatocytes (Hep) were used as positive control of urea cycle enzymes (Figure 11 A-E).

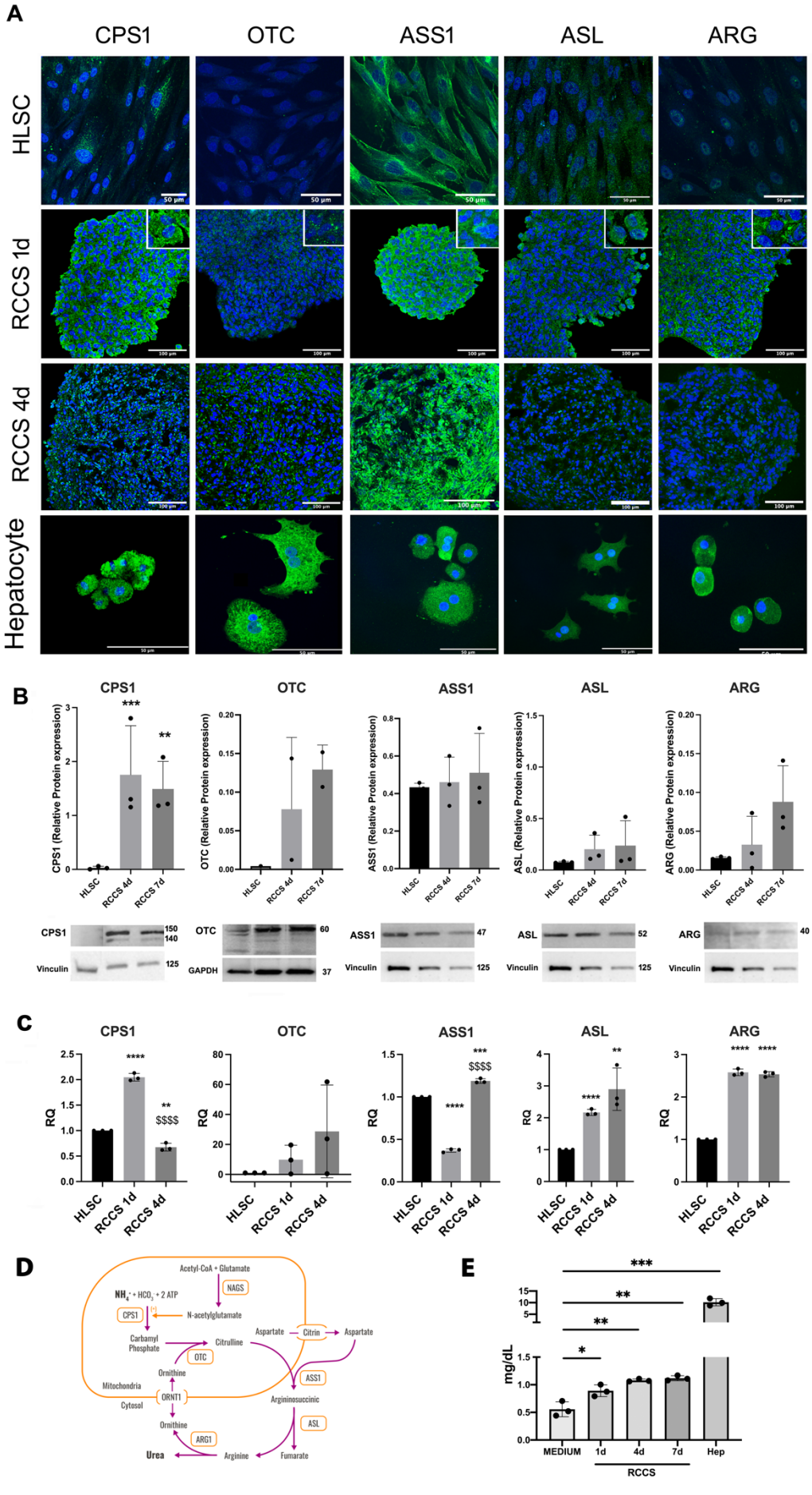
A
CPS1
OTC
ASS1
ASL
ARG
HLSC
RCCS 1d
RCCS 4d
Hepatocyte
B
CPS1
OTC
ASS1
ASL
ARG
CPS1 (Relative Protein expression)
OTC (Relative Protein expression)
ASS1 (Relative Protein expression)
ASL (Relative Protein expression)
ARG (Relative Protein expression)
HLSC
RCCS 4d
RCCS 7d
CPS1
Vinculin
OTC
GAPDH
ASS1
ASL
ARG
C
RQ
HLSC
RCCS 1d
RCCS 4d
D
Acetyl-CoA + Glutamate
NAGS
N-acetylglutamate
CPS1
Carbamyl Phosphate
Citrulline
OTC
Ornithine
Mitochondria
Cytosol
ORNT1
Aspartate
Citrin
ASS1
Argininosuccinic
ASL
Fumarate
Arginine
ARG1
Urea
E
mg/dL
MEDIUM
1d
4d
7d
Hep
RCCS

Figure 11: Expression of urea cycle enzymes. (A) Representative immunofluorescence micrographs of the urea cycle enzymes CPS1, OTC, ASS1, ASL and ARG in HLSCs and differentiated HLSCs in RCCS after 1 and 4 days. Human hepatocyte cells were used as positive control. Scale bar, 50 and 100 µm, magnification × 40, insert pictures. Nuclei are stained in blue with DAPI. **(B)** Representative blot and relative amounts of proteins counted in relation to HLSC. The results are presented as mean values of three independent experiments and are normalized using Vinculin and GAPDH as housekeeping proteins ±SD. ***p< 0.001 RCCS 4d vs. HLSC, **p< 0.01 RCCS 7d vs. HLSC. **(C)** Real-time PCR array data of urea cycle enzyme genes in HLSCs and differentiated HLSCs. Results were normalized using TBP and undifferentiated HLSCs were used as experimental control. Data are expressed as Relative Quantification (RQ) of five independent experiments ±SD. *p< 0.05, **p< 0.01, ***p< 0.001,****p< 0.0001 RCCS 1d and RCCS 4d vs. HLSC, p< 0.0001 RCCS 4d vs. RCCS 1d. (**D**) Schematic representation of Urea cycle. Created with Biorender.com (**E**) Urea into the supernatant of differentiated HLSC in RCCS after 1, 4, 7 days and human hepatocytes after 4 days in RCCS was quantified by Quantichrom assay kit. Results were expressed as mg/dL of urea. The results are presented as mean values obtained from three independent experiments ±SD * p<0.05, ** p<0.01, *** p<0.001 HLSC cultured in RCCS 1d, 4d, 7d and human hepatocyte (Hep) vs. medium along.

Stem cell marker modulation of hepatocyte-like HLSCs differentiated in RCCS

NANOG, KLF4, OCT 3/4 and Sox2 are key markers used to define stem cell identity [54]. In order to evaluate the modulation of these markers during the differentiation, we performed immunofluorescence staining on HLSCs differentiated cells over a period of 7 days. As shown in the figure 12A, immunofluorescence analysis revealed that NANOG, KLF4, and OCT3/4 exhibited a cytoplasmic localization during differentiation, in contrast to their nuclear localization in undifferentiated HLSCs (Figure 5D). SOX2, however, remained predominantly nuclear throughout the differentiation process. The mRNA expression analysis demonstrated a consistent decrease in KLF4 expression at all time points. In contrast, NANOG, OCT3/4, and SOX2 showed an initial upregulation, with peak expression observed on day 4, followed by a decline by day 7 (Figure 12 B).

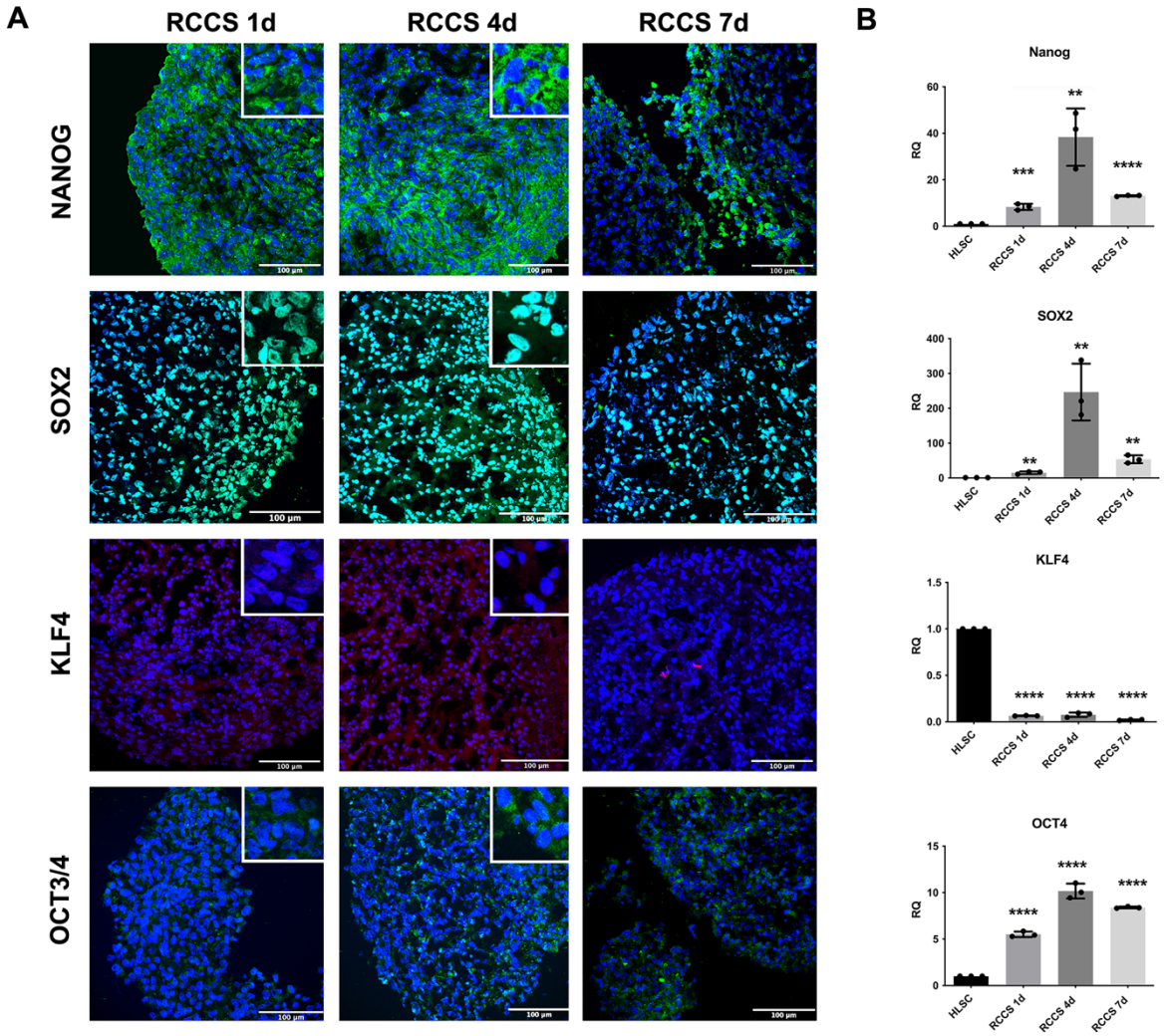

Figure 12: Stem cell markers. (A) Representative immunofluorescence micrograph of stem cell markers Nanog, SOX2, KLF4, OCT3/4 in undifferentiated HLSCs and RCCS differentiated HLSCs. Scale bar, 100µm; magnification 40X, insert pictures. Nuclei are stained in blue with DAPI. (B) Real-time PCR of the embryonic stem cells genes. Results were normalized using TBP and undifferentiated HLSCs were used as control. Results are expressed as Relative Quantification (RQ). The results are presented as mean values of five independent experiments ±SD. * $p<0.05$, * $p<0.01$, * $p<0.001$, * $p<0.0001$ RCCS 1d and 4d vs HLSC.

Indocyanine green (ICG) uptake by hepatocyte-like HLSCs differentiated in RCCS

Indocyanine green (ICG) is an anionic dye used to evaluate liver function in clinic [55]. Currently, ICG clearance has been proposed to define patients with a risk of developing postoperative liver dysfunction [56]. We developed an *in vitro* assay to measure ICG uptake in differentiated HLSC aggregates (Figure 13A). As shown in Figures 13B and C, ICG uptake was significantly higher in HLSCs after four days of differentiation compared to both undifferentiated HLSCs and HaCaT cell aggregates (negative control), which served as a negative control. ICG uptake is facilitated by the

organic anion transporting polypeptide (OATP) transporter, commonly associated with mature hepatocytes [57]. To investigate the role of OATP1B1 expression during HLSC differentiation, we performed immunofluorescence and real-time PCR analyses on HLSC aggregates compared to undifferentiated cells. OATP1B1 expression was significantly upregulated after one day of differentiation and increased further after four days, compared to undifferentiated HLSCs, with human hepatocytes used as a positive control (Figures 13D, E). To evaluate the degree of hepatic differentiation in HLSCs, we compared OATP1B1 mRNA expression (a marker of mature hepatocytes) in differentiated HLSCs and human hepatocytes. Our data demonstrated that OATP1B1 mRNA expression in differentiated HLSCs was lower than in human hepatocytes (Figure 13E), indicating that differentiated HLSCs are partially committed to a mature hepatocyte phenotype.

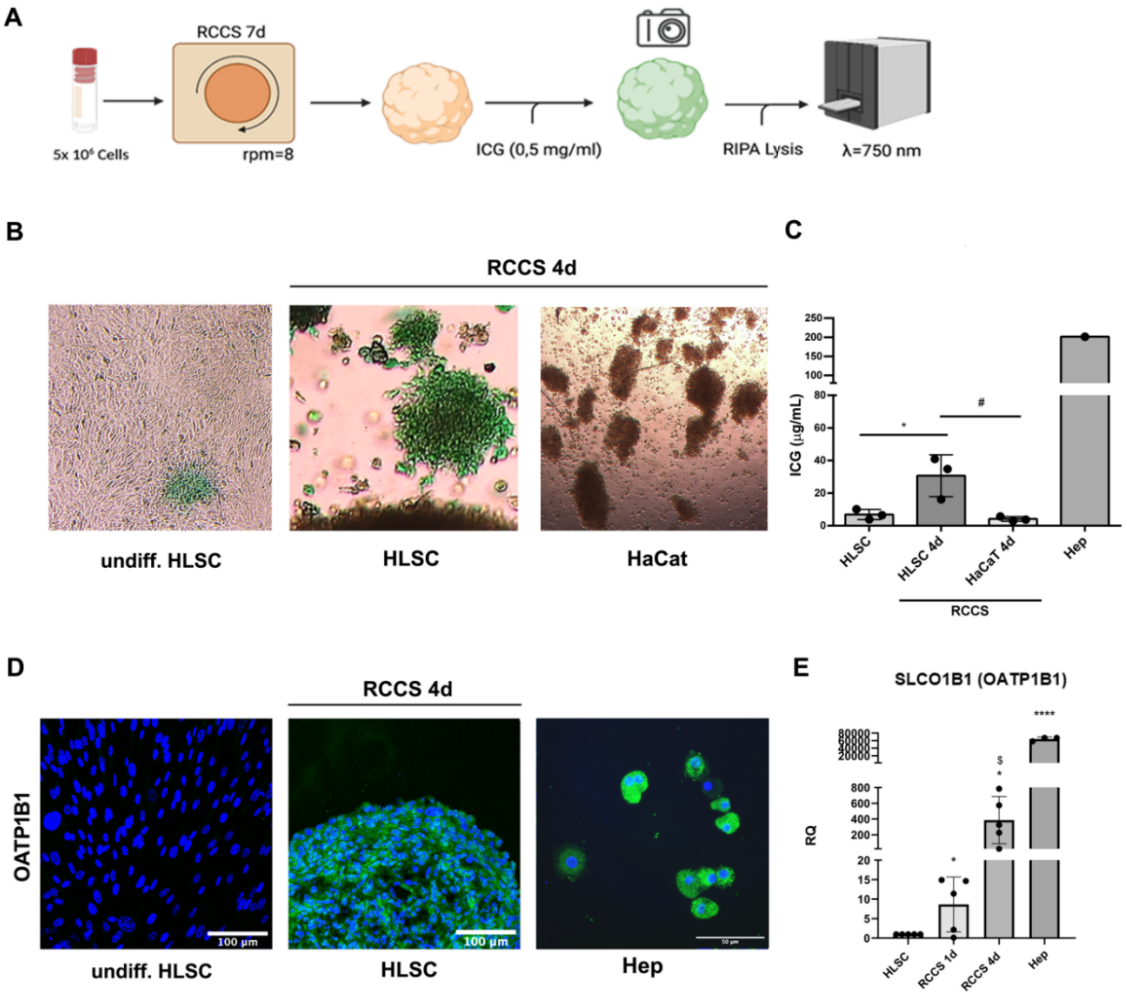

Figure 13: Indocyanine green (ICG) update assay. (A) Schematic representation of the assay. Created with Biorender.com. (B) Representative micrographs of undifferentiated, differentiated HLSCs and HaCat showing uptake of ICG after 1 h × 4 magnification. (C) ICG quantification in undifferentiated HLSCs, HLSCs, HaCaT and human hepatocyte (Hep) after 4 days in RCCS. Data were measured at 750 nm optical density. *$p< 0.05$, HLSCs RCCS 4d vs. undifferentiated HLSCs; $^{\#}p< 0.05$ HLSCs RCCS 4d vs. HaCaT RCCS 4d. (D) Representative immunofluorescence micrograph of OATP1B1 in HLSCs, RCCS differentiated HLSCs and human hepatocyte (Hep) at day 4. Human hepatocytes were used as positive control. Nuclei are stained in blue with DAPI. Scale bar, 50 and 100 µm, ×40 magnification. (E) Real time PCR data of OATP1B1 (SLCO1B1) in HLSC, HLSC differentiated after 1 and 4 days, and human hepatocyte (Hep). Results were normalized using TBP and undifferentiated HLSCs were used as experimental control. Data are expressed as Relative Quantification (RQ) ±SD of five independent experiments. *$p< 0.05$, RCCS 1d and RCCS 4d vs. HLSC; $^{\$}p< 0.05$ RCCS 1d vs. RCCS 4d, ****$p< 0.0001$ Hep vs. HLSC.

Discussion

In this study, we proposed a 3D rotary cell culture system to explore the potential differentiation ability of HLSCs, focusing on both gene expression and functional assays to confirm the hepatic-like characteristics of differentiated cells.

Over the past decade, differentiation strategies for hepatocyte-like cells have been extensively studied, leading to straightforward and reproducible protocols [58,59]. The differentiation process typically involves three stages: differentiation into definitive endoderm, hepatoblast differentiation, and finally, hepatocyte maturation. *In vitro* systems allow researchers to replicate and study these processes in depth through two main approaches, generating hepatocyte-like cells in either 2D or 3D culture formats. Even though 2D culture is widely used to study differentiation into hepatocyte-like cells, the microenvironment lacks physical cues from the extracellular matrix (ECM) that influence cell behavior. To address this limitation, 3D cultures systems have been studied, such as scaffold-based or spheroid cultures, with the aim of promoting cell–cell interactions and functionality that more closely mimic *in vivo* conditions [60,61]. Therefore, 3D approach mimics liver organogenesis process [62]. Studies have shown that stem cells cultured in 3D systems, such as embryoid bodies, spheroids, or scaffolds, differentiate into hepatocyte-like cells more efficiently than those cultured in 2D method [61]. Moreover, the combination of 3D structure and differentiation factors, including specific cytokines, vitamin and hormones such as HGF, FGF4, ascorbic acid, oncostatin M and dexamethasone, have proved to be pivotal element in hepatocyte-like lineage generation [41,63-65]. Ogawa et al. demonstrated that the combination of these factor with 3D approach directed the maturation of hESCs into hESC-derived hepatocyte-like cells [66].

In a 3D *vs* 2D comparative study, the authors demonstrated that rotary cell culture systems (RCCS) can generate homogenous hepatocyte-like cells from hiPSCs. These cells expressed mature hepatocyte markers (CYP1A2, CYP2D6, and alpha-1 antitrypsin) and were positive for albumin,

suggesting that RCCS provides a more suitable microenvironment for hepatocyte maturation than 2D culture condition [61].

HLSCs have previously demonstrated the potential to differentiate into hepatocyte-like cells, in bioartificial liver devices, liver scaffolds and RCCS [24,47,48]. Bioartificial liver device culture system highlight the HLSCs capacity to differentiate into hepatic-like cells analyzing secreted HGF, albumin and urea at levels similar to hepatocytes [47]. In the decellularized liver scaffold model, Navarro-Tableros et al. evaluated the lactate dehydrogenase and three subtypes of cytochrome P450 in HLSCs differentiated cells [48]. In addition, they further confirm the hepatic -like commitment by the detection of urea suggesting that HLSCs had acquired a metabolic activity similar to hepatocytes [48]. However, these methods often require a large number of cells and extended differentiation times, which limit their applicability or large-scale production settings. Our approach reduces these requirements by enabling characterization with 5×10^6 cells, a significant reduction of cell compared to other models, respectively 300×10^6 for bioartificial liver devise and $80–100 \times 10^6$ for liver scaffold recellularization. Therefore, our study achieves measurable differentiation markers within a shorter timeframe (up to 4 days of differentiation) employing a reduced number of cells.

In this study, we combined several methods to better characterize the differentiation capabilities of HLSCs and determine the optimal time frame for analyzing different parameters. At day 7 of culture, we observed a high percentage of apoptotic cells, especially in the core of the cell aggregates. This could be due to nutrient exhaustion and/or lack of oxygen supply (especially to the core of the aggregates) within the rotary culture vessel as the number of days of differentiation increased. This finding aligns with the challenges faced in maintaining optimal conditions in dense 3D structures, where oxygen and nutrient gradients can lead to hypoxic zones and cell death. Such gradients may contribute to the observed transient upregulation of pluripotency markers (e.g., Nanog, OCT3/4, SOX2, and KLF4), which are known to respond to low oxygen conditions [67-69]. Interestingly, we observed that Nanog and OCT3/4 translocated during differentiation, potentially as a

mechanosensitive response to the continuous movement in our 3D culture system, similar to previous findings on mechanosensitive factors in stem cell differentiation [70,71]. Thus, we hypothesize that the reduced oxygen levels experienced by HLSCs within the differentiated aggregates may have contributed to the observed transient upregulation of these pluripotency markers.

Various stage-specific marker can be assessed such as gene expression to define the stem cell differentiation process into hepatocyte-like cells (HLCs). In addition, *in vitro* functional tests may confirm the fully differentiation process [58,59]. In our current study, we demonstrated that differentiated HLSCs showed a significant upregulation of key gene markers characteristic of mature hepatocytes compared to undifferentiated HLSCs. Of note, cytochrome P450 isoenzymes (CYP1A1, CYP1A2, CYP1B1, CYP2B6, CYP3A4, CYP3A7, and CYP7A1), as well as two enzymes crucial for the excretion of endobiotic and xenobiotic compounds (UGT1A3 and UGT1A4) were upregulated and the organic anion-transporter polypeptide of the OATP family involved in the hepatic uptake of several drugs (OATP1B1), SERPINA1, FVIII. We also observed a gene expression modulation of transcription factors involved in liver embryological development, such as four members of HNF family and CEBPB and a reduction of αFP expression. Furthermore, our HLSCs differentiated cells exhibit a significant expression of four enzymes of the urea cycle (CPS1, OTC, ARG1, and ASL), confirmed by the secretion of Urea using MS/MS analysis. Given the expression of OATP1B1 on the membrane of differentiated HLSCs, we developed a quantitative in vitro assay to measure the functional uptake of indocyanine green (ICG) post-differentiation. Furthermore, we confirmed functionality the secretion factor VIII into the supernatant after differentiation.

Mature hepatocytes play a critical role in the coagulation cascade, producing and secreting coagulation factor VIII (FVIII), an essential protein for blood clotting [72]. Pettinato et al. demonstrated the coagulation potential of hepatic-like organoids, derived from cocultured iPS and endothelial cells, by showing peak secretion of FVIII and FX into the conditioned medium after 6 days of differentiation. In our 3D model, we observed robust secretion of FVIII from hepatic-

committed HLSCs as early as day 1, persisting through the 4-day differentiation period. Noteworthy, we detect two cleavage versions of FVIII into the supernatant, mirroring the mature FVIII expression in human hepatocytes.

To further evaluate the HLSCs differentiation, we assessed and ICG assay. ICG assay is a commonly used method for evaluating liver functionality and clearance *in vitro* and clinical setting [73]. The clearance ability of the liver cells is the based strategy to evaluate the amount of ICG excreted from circulation into the bile. Human hepatocytes, main actors in this process, have a distinct pattern of ICG uptake and release. Measurement of its clearance make it suitable for a number of potential applications in liver transplantation including assessment of liver function and real-time assessment donor graft quality before procurement and graft metabolic function before transplant [74]. Indeed, hepatocytes ICG take up may be detected in 30 min and then excrete the unchanged dye after 1–2 h [55]. Of note, the hepatocyte-specific transporter OATP1B1 mediates this mechanism, making it an ideal target molecule for testing the hepatocyte-like properties of differentiated HLSCs. In this study, we designed a specific easy assay that aim to quantify the amount of ICG uptake by differentiated HLSCs. Moreover, we correlated ICG uptake to the expression of OATP1B1, confirming their hepatocyte-like functional similarity.

Conclusions

In this published study (DOI: 10.3389/fcell.2024.1352013), we demonstrated that HLSCs progressively upregulated a broad range of hepatic markers and functions from day 1 to day 4 of differentiation *in vitro* 3D system upon specific stimuli. These markers included liver-specific genes, urea cycle enzymes, cytochrome P450 enzymes, transmembrane transporters, and coagulation factors. Furthermore, hepatocyte-like functional activity in differentiated HLSC aggregates was confirmed in vitro by urea and FVIII secretion, as well as indocyanine green (ICG) uptake—mediated by increased expression of the related anionic transporter after differentiation.

This work provides a delved characterization of a 3D *in vitro* system, establishing its potential as a potency assay for evaluating the final GMP-grade HLSC cell therapy product using urea quantification or an ICG assay. We propose a matrix approach that integrates multiple methods to assess the differentiation status of HLSC aggregates, from which a quantitative validation assay can be selected for future use. Furthermore, our approach is rapid and straightforward to implement in a GMP context, facilitating transfer to GMP environments and supporting standardization efforts.

Future prospective

This published work highlights the characteristics of HLSCs at baseline with a commitment to both stem and hepatocyte phenotypes, while during differentiation into hepatocyte-like cells, demonstrating the ability to progressively acquire markers that more strongly characterize hepatocytes. As previously shown by our group, HLSCs represent an excellent tool for treating liver diseases through paracrine action but also by differentiating into hepatocytes. This study emphasizes the potential of HLSCs to differentiate into hepatocytes when subjected to a microenvironment that presents the same hepatocyte growth factors and is stimulated by a 3D structure.

From a clinical perspective, this study proposes a multi-assay approach to validate a GMP product as a potency assay and demonstrate the capability of the product. Indeed, after the Phase I clinical trial of HLSC, where the main aim was to demonstrate the safety of HLSCs cell therapy in a setting of liver genetic disorders. Here we demonstrated the capability to differentiate into hepatocyte-like cells, which represents a pivotal aim for a future Phase II clinical trial, as requested by major drug agencies such as European medicines agency (EMA) and USA food and drug agency (FDA).

Moreover, this study opens up to further investigation in a pre-clinical setting. First, further studies may implement HLSC characterization by modifying cell culture conditions. It may also be interesting to combine different cell types to generate organoids and evaluate their function. Therefore, these tools could empower the understanding of HLSC differentiation and set up other different functional assays such as toxicology studies using different drugs. In a setting of gene therapy studies in urea cycle liver disease, HLSC aggregates might be used to evaluate the level of urea produced upon gene therapy, in combination with differentiation protocol. Noteworthy, 3D cell cultures, may also represent a surrogate for animal model as fast valid alternative tool to enhance the value of preclinical in vitro investigations. Of note, during my PhD program, I began to investigate the gene therapy approach in a cell therapy setting using HLSCs (as reported in Appendix 1).

Abbreviation

HLSCs: Human liver stem cells

RCCS: rotary cell culture system

HLCs: Hepatocyte-like cells

qRT-PCR: Quantitative reverse transcription PCR

GMP: good manufacturing product

ALF: acute liver failure

ESLD: end-stage liver disease

NASH: Non-alcoholic steatohepatitis

3D: three-dimensional

BAL: bioartificial liver

ALI: acute liver injury

MCB: master cell bank

WCB: working cell bank

AIFA: Agenzia Italiana del farmaco

DMEM: Dulbecco's Modified Eagle Medium

hrEGF: human recombinant epidermal growth factor

hrFGF2: human recombinant fibroblast growth factor basic 2

LA-BSA: linoleic acid-bovine serum albumin

ITS: insulin-transferrin-selenium

FGF2: fibroblast growth factors 2

FGF4: fibroblast growth factors 4

BMP4: Bone morphogenetic protein 4

OSM: Oncostatin M

ITS: insulin- transferrin- selenium

ESCs: Embryonic stem cells

iPSCs: Induced pluripotent stem cells

HSCs: Hematopoietic stem cells

G-CSF: granulocyte-colony stimulating factor

MSCs: Mesenchymal stromal cells

HGF: Hepatocyte growth factor

VEGF: Vascular endothelial growth factor

HNF4: Hepatocyte Nuclear Factor 4

ALB: albumin

CK 8: cytokeratin 8

CK 18: cytokeratin 18

IL: interleukin

αFP: alpha-fetoprotein

A1AT: alpha-1-antitrypsin

FLF: fulminant liver failure

CYP450: Cytochrome P 450

OCT: Optimal cutting temperature

OCT3/4: Octamer binding transcription factor ¾

Sox2: sex-determining region Y-box 2

KLF4: Krüppel-like factor 4

OTC: Ornithine transcarbamylase

ASS1: Argininosuccinate synthase 1

CPS1: Carbamoyl-phosphate synthase 1

ARG1: Arginase1

ASL: Argininosuccinate lyase

FVIII: Coagulation factor VIII

TUNEL: Terminal dUTP nick end-labeling

PAS: Periodic acid Schiff

LC-MS/MS: Liquid chromatography hyphenated with tandem mass spectrometry

HILIC: hydrophilic interaction liquid chromatography

Ppm: parts per million

CPD: cumulative population doubling

PCNA: proliferating cell nuclear antigen

Hep: Human hepatocytes

ICG: Indocyanine green

OATP: organic anion transporting polypeptide

UGT1A1: UDP glucuronosyltransferase 1 family, polypeptide A1

UGT1A3: UDP glucuronosyltransferase 1 family, polypeptide A3

UGT1A4: UDP glucuronosyltransferase 1 family, polypeptide A4

POUF5F1: POU class 5 homeobox 1

SOX17: SRY (sex determining region Y)-box 17

FOXA2: Forkhead box A2

KRT8: Keratin 8

KRT18: Keratin 18

KRT19: Keratin 19

CEBPA: CCAAT/enhancer binding protein (C/EBP), alpha

CEBPB: CCAAT/enhancer binding protein (C/EBP), beta

HNF1A: HNF1 homeobox A

HNF1B: HNF1 homeobox B

HNF4A: Hepatocyte nuclear factor 4, alpha

ONECUT: One cut homeobox 1

SERPINA1: Serpin peptidase inhibitor, clade A (alpha-1 antiproteinase, antitrypsin), member 1

PAH: Phenylalanine hydroxylase

CYP1A1: Cytochrome P450, family 1, subfamily A, polypeptide 1

CYP1A2: Cytochrome P450, family 1, subfamily A, polypeptide 2

CYP1B1: Cytochrome P450, family 1, subfamily B, polypeptide 1

CYP2B6: Cytochrome P450, family 2, subfamily B, polypeptide 6

CYP2C9: Cytochrome P450, family 2, subfamily C, polypeptide 9

CYP3A4: Cytochrome P450, family 3, subfamily A, polypeptide 4

CYP3A7: Cytochrome P450, family 3, subfamily A, polypeptide 7

CYP7A1:Cytochrome P450, family 7, subfamily A, polypeptide 1

ACTB: Actin, beta

B2M: Beta-2-microglobulin

HPRT1: Hypoxanthine phosphoribosyltransferase 1

GAPDH: Glyceraldehyde-3-phosphate dehydrogenase

GUSB: Glucuronidase, beta

RTC: Reverse Transcription Control

PPC: Inter Plate Reproducibility Control

HGDC: Human Genomic DNA Contamination

Appendix 1

During my PhD, the research activity has been mainly focused on research projects that aimed to study the adult stem cell ability as a promising cell therapy in liver regenerative medicine. In our group we have been mainly concentrated on human liver stem cells (HLSCs) and we deeply characterized the hepatic-like differentiation in a 3D model using a multi-assay approach. Our research lead our group to publish this work (DOI: 10.3389/fcell.2024.1352013) and submit a patent for the indocyanine green (ICG) quantification as a novel assay to quantify the uptake of ICG in 3D model (**n° 23201384.7- A method of validating as pharmaceutically active a batch of undifferentiated adult stem cells having the potential to differentiate along the hepatic lineage**).

HLSCs have demonstrated significant regenerative potential in various preclinical liver diseases, including acute and chronic liver disease models, and mouse genetic disorders. Furthermore, a Phase I clinical trial conducted in Turin highlighted the safety profile of this cell therapy and its ability to improve liver function as a bridge therapy for patients with urea cycle disorders.

Our group has previously shown that HLSCs can ameliorate Crigler-Najjar syndrome type I in mice. Additionally, HLSCs-derived extracellular vesicles have proven to compensate for ASS1 deficiency by delivering ASS1 mRNA and enzyme in type I citrullinemia. These promising results have led our group to explore a combination of cell and gene therapy to treat liver genetic disorders.

In collaboration with the transplantation center at Turin Molinette Hospital, we have established a cell bank encompassing various liver genetic disorders. Among these, we have isolated HLSCs from a patient with OTC X-linked deficiency. We have developed an in vitro model of HLSCs overexpressing OTC as a proof-of-concept for treating OTC deficiency. In collaboration with the Cantore group (San Raffaele Hospital), we generated OTC-transduced HLSCs using a lentiviral vector with a ubiquitous phosphoglycerate kinase (PGK) promoter (Figure 14 A). Our preliminary results demonstrate efficient transduction of HLSCs with a high expression of GFP (over 80%) at an MOI of 100 (Figure 14 B, C), without *in vitro* toxicity side effect (data not shown). Subsequently,

HLSCs were transduced with the PGK.OTC vector. Both at passage 11 and 13, PGK.OTC HLSCs exhibited increased levels of OTC gene expression, confirming lentviral transduction efficiency (Figure 14 E). Immunofluorescence and Western blot analyses further confirmed the expression of the OTC protein (Figure 14 F, G). To evaluate mitochondrial localization of overexpressed OTC, we co-stained the enzyme of interest with a mitochondrial dye (Figure 14 F). Overall, our preliminary results provide a proof-of-concept for generating a valuable tool to correct OTC deficiency. Further investigations are required to assess the enzymatic activity of the transduced enzyme and the urea production rate. In a clinical setting, this strategy could be employed to treat patients with urea cycle disorders using an autologous approach, involving engineered human liver stem cells; thus, providing a promising alternative to liver transplantation.

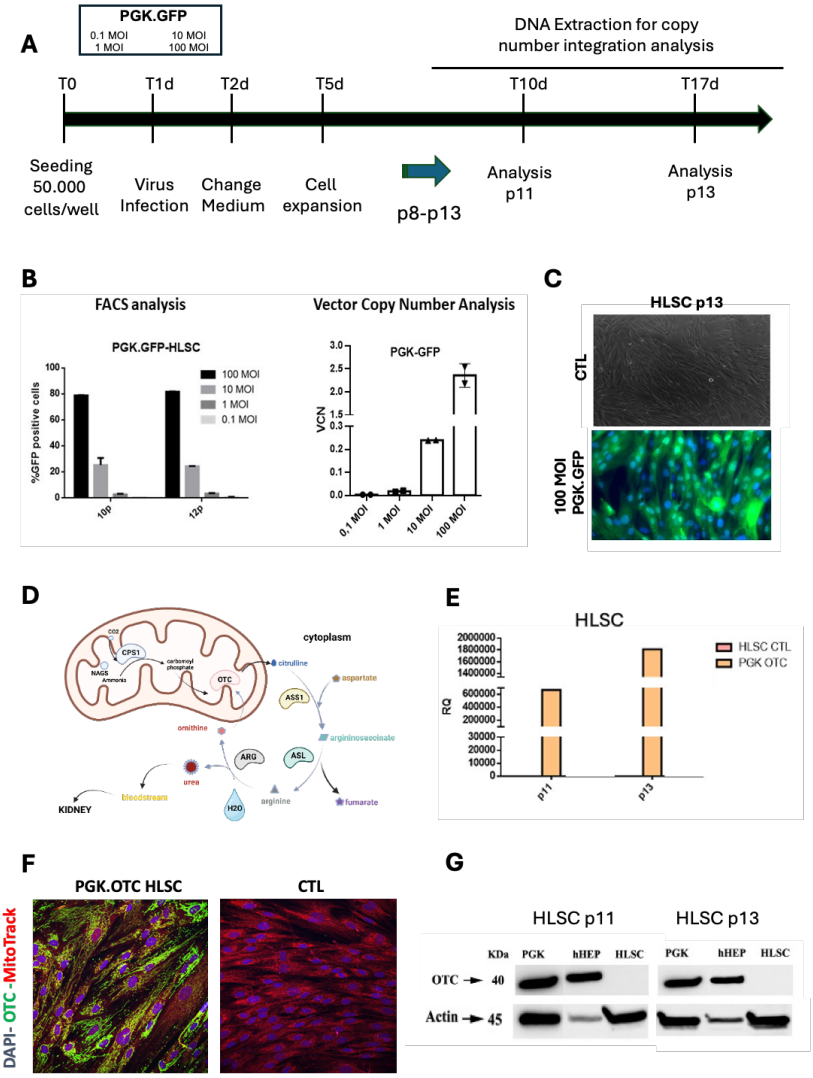

Figure 14: Generation of transduced PGK.OTC HLSC. (A) Schematic experimental lentiviral transduction schedule of HLSC. (B) GFP FACS analysis quantification of HLSC transduced with PGK.GFP at different multiplicity of infection (MOI- ratio of virus to cell). Quantification of vector copy number analysis (VCN) integrated in the HLSC genome. (C) Combination of fluorescent-Brierfield image to detect the GFP after lentiviral transduction at 100 MOI. Untransduced (CTL) cells were used as a negative control. (D) Schematic representation of Urea cycle. Created with Biorender.com. (E) Real time PCR data of OTC in HLSC, PGK.OTC HLSC. Results were normalized using TBP and untransduced HLSCs were used as experimental control. HLSC were analyzed at both passage 11 and 13. (F) Representative immunofluorescence micrograph of OTC in untransduced HLSCs (CTL) and PGK.OTC HLSCs. Nuclei were stained with DAPI. Mitochondria were stained with MitoTrack -red dye. (G) Representative blot of untransduced HLSCs, PGK.OTC HLSC and hepatocyte (hep) as a positive control. Actin was used as Houskeeping.

During my PhD experience, I had the opportunity to investigate the role of extracellular vesicles (EVs) derived from adult stem cell in regenerative medicine field which have been also published in international journals. One of the first projects (Figure 15) regards the study of the therapeutic potential of EVs derived from mesenchymal stem cell in a corneal wound healing murine model. The administration two doses of bone marrow MSC-EVs modulate corneal repair dynamics and are promising as a new cell-free approach for intervening on burn wounds, especially in the avascularized region of the eye.

Open Access Article

Bone Marrow Mesenchymal Stromal/Stem Cell-Derived Extracellular Vesicles Promote Corneal Wound Repair by Regulating Inflammation and Angiogenesis

by Gabriele Saccu [1,†], Valeria Menchise [2,†], Chiara Gai [3], Marina Bertolin [4], Stefano Ferrari [4], Cristina Giordano [5], Marta Manco [1], Walter Dastrù [1], Emanuela Tolosano [1], Benedetta Bussolati [1], Enzo Calautti [1], Giovanni Camussi [3], Fiorella Altruda [1,*] and Sharmila Fagoonee [2,*]

[1] Molecular Biotechnology Center "Guido Tarone", Department of Molecular Biotechnology and Health Sciences, University of Turin, 10126 Turin, Italy
[2] Institute of Biostructure and Bioimaging, National Research Council (CNR), Molecular Biotechnology Center "Guido Tarone", 10126 Turin, Italy
[3] Department of Medical Sciences, University of Turin, 10126 Turin, Italy
[4] Veneto Eye Bank Foundation (FBOV), 30174 Venice, Italy
[5] Ophthalmology Veterinary Practice, C.so Galileo Ferraris 121, 10126 Turin, Italy
* Authors to whom correspondence should be addressed.
† These authors contributed equally to this work.

Cells **2022**, *11*(23), 3892; **https://doi.org/10.3390/cells11233892**

Submission received: 27 October 2022 / Revised: 22 November 2022 / Accepted: 28 November 2022 / Published: 2 December 2022

(This article belongs to the Collection **Exclusive Papers from Editorial Board Members and Invited Scholars in *Cells***)

Download Browse Figures Versions Notes

Abstract

Severe corneal damage leads to complete vision loss, thereby affecting life quality and impinging heavily on the healthcare system. Current clinical approaches to manage corneal wounds suffer from severe drawbacks, thus requiring the development of alternative strategies. Of late, mesenchymal stromal/stem cell (MSC)-derived extracellular vesicles (EVs) have become a promising tool in the ophthalmic field. In the present study, we topically delivered bone-marrow-derived MSC-EVs (BMSC-EVs), embedded in methylcellulose, in a murine model of alkali-burn-induced corneal damage in order to evaluate their role in corneal repair through histological and molecular analyses, with the support of magnetic resonance imaging. Our data show that BMSC-EVs, used for the first time in this specific formulation on the damaged cornea, modulate cell death, inflammation and angiogenetic programs in the injured tissue, thus leading to a faster recovery of corneal damage. These results were confirmed on cadaveric donor-derived human corneal epithelial cells in vitro. Thus, BMSC-EVs modulate corneal repair dynamics and are promising as a new cell-free approach for intervening on burn wounds, especially in the avascularized region of the eye.

Keywords: extracellular vesicles; cornea; MRI; Gd-AAZTA-MADEC; methylcellulose; mesenchymal stromal/stem cells; Esrp1

Figure 15: Abstract of the paper Saccu G et al. Bone Marrow Mesenchymal Stromal/Stem Cell-Derived Extracellular Vesicles Promote Corneal Wound Repair by Regulating Inflammation and Angiogenesis. Cells **2022**, 11(23), 3892; **https://doi.org/10.3390/cells11233892**

In the context of EVs, we characterized and evaluated the role of aqueous humor (AH) derived EVs. We provided evidence, of the possible AH-EV origin from stromal cells, limbal epithelial/stem cells, ciliary epithelium and corneal endothelium. In addition, we showed their *in vitro* proliferative and regenerative capacities (Figure 16).

Research article

Phenotypic and functional characterization of aqueous humor derived extracellular vesicles

Roberta Verta [a,1], Gabriele Saccu [b,1], Adele Tanzi [a,1], Cristina Grange [b], Lola Buono [a], Sharmila Fagoonee [c], Maria Chiara Deregibus [d], Giovanni Camussi [b], Simona Scalabrin [e], Raffaele Nuzzi [e,2], Benedetta Bussolati [a,*,2]

[a] Department of Molecular Biotechnology and Health Sciences, University of Torino, Italy
[b] Department of Medical Sciences, University of Torino, Torino, Italy
[c] Institute of Biostructure and Bioimaging, National Research Council, Molecular Biotechnology Center, Turin, Italy
[d] 2i3T Business Incubator and Technology Transfer, University of Torino, Italy
[e] Department of Surgical Sciences, University of Torino, Italy

ARTICLE INFO

Keywords:
Extracellular vesicles
Exosomes
Wound healing
Limbal stem cells
Corneal epithelium

ABSTRACT

Extracellular vesicles (EVs) are double membrane vesicles, abundant in all biological fluids. However, the characterization of EVs in aqueous humor (AH) is still limited. The aim of the present work was to characterize EVs isolated from AH (AH-EVs) in terms of surface markers of cellular origin and functional properties. We obtained AHs from patients with cataract undergoing surgical phacoemulsification and insertion of intraocular lenses (n = 10). Nanoparticle tracking analysis, electron microscopy, super resolution microscopy and bead-based cytofluorimetry were used to characterize EVs from AH. Subsequently, we investigated the effects of AH-EVs on viability, proliferation and wound healing of human immortalized keratinocyte (HaCaT) cells *in vitro* in comparison with the effect of mesenchymal stromal cell-EVs (MSC-EVs). AH-EVs had a mean size of around 100 nm and expressed the classical tetraspanins (CD9, CD63 and CD81). Super resolution microscopy revealed co-expression of CD9, CD63 and CD81. Moreover, cytofluorimetric analysis highlighted the expression of mesenchymal, stem, epithelial and endothelial markers. In the *in vitro* wound healing assay on HaCaT cells, AH-EVs induced a significantly faster wound repair, comparable to the effects of MSC-EVs, and promoted HaCaT cell viability and proliferation. We provide evidence, herein, of the possible AH-EV origin from stromal cells, limbal epithelial/stem cells, ciliary epithelium and corneal endothelium. In addition, we showed their *in vitro* proliferative and regenerative capacities.

Figure 16: Abstract of the paper Verta R, Saccu G. and Tanzi A et al. Phenotypic and functional characterization of aqueous humor derived extracellular vesicles. doi: 10.1016/j.exer.2023.109393

In a commentary, we briefly summarized the novel stem cell-based approaches to face corneal regeneration embracing the use of adult stem cell and stem cell derived extracellular vesicles (Figure 17).

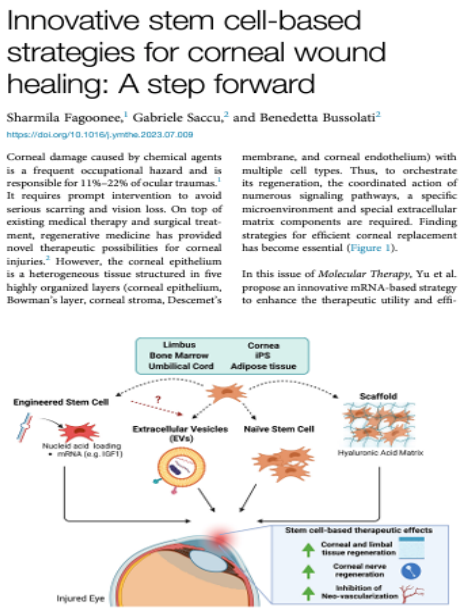

Innovative stem cell-based strategies for corneal wound healing: A step forward

Sharmila Fagoonee,[1] Gabriele Saccu,[2] and Benedetta Bussolati[2]

https://doi.org/10.1016/j.ymthe.2023.07.009

Corneal damage caused by chemical agents is a frequent occupational hazard and is responsible for 11%–22% of ocular traumas.[1] It requires prompt intervention to avoid serious scarring and vision loss. On top of existing medical therapy and surgical treatment, regenerative medicine has provided novel therapeutic possibilities for corneal injuries.[2] However, the corneal epithelium is a heterogeneous tissue structured in five highly organized layers (corneal epithelium, Bowman's layer, corneal stroma, Descemet's membrane, and corneal endothelium) with multiple cell types. Thus, to orchestrate its regeneration, the coordinated action of numerous signaling pathways, a specific microenvironment and special extracellular matrix components are required. Finding strategies for efficient corneal replacement has become essential (Figure 1).

In this issue of *Molecular Therapy*, Yu et al. propose an innovative mRNA-based strategy to enhance the therapeutic utility and effi-

Figure 17: Commentary: Fagoonee S, Saccu G, Bussolati B. Innovative stem cell-based strategies for corneal wound healing: A step forward. Mol Ther. 2023;31(8):2307-2308. doi:10.1016/j.ymthe.2023.07.009

During my PhD experience, I had the opportunity to produce three reviews; one of which gives an overview of the application of natural or engineered EVs isolated from stem cells to treat different kidney pathologies (Figure 18).

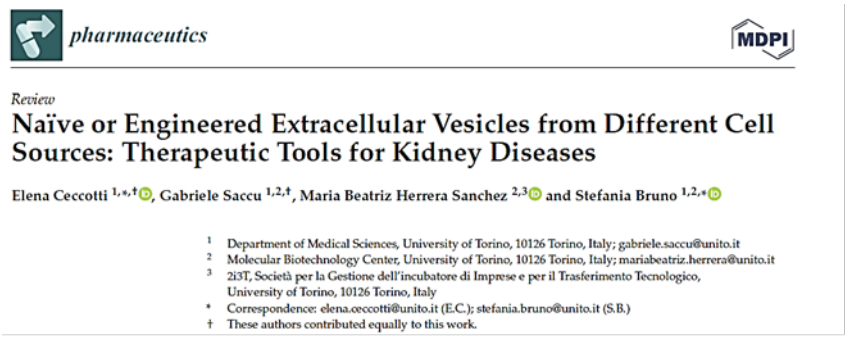

pharmaceutics MDPI

Review

Naïve or Engineered Extracellular Vesicles from Different Cell Sources: Therapeutic Tools for Kidney Diseases

Elena Ceccotti [1,*,†], Gabriele Saccu [1,2,†], Maria Beatriz Herrera Sanchez [2,3] and Stefania Bruno [1,2,*]

[1] Department of Medical Sciences, University of Torino, 10126 Torino, Italy; gabriele.saccu@unito.it
[2] Molecular Biotechnology Center, University of Torino, 10126 Torino, Italy; mariabeatriz.herrera@unito.it
[3] 2i3T, Società per la Gestione dell'incubatore di Imprese e per il Trasferimento Tecnologico, University of Torino, 10126 Torino, Italy
* Correspondence: elena.ceccotti@unito.it (E.C.); stefania.bruno@unito.it (S.B.)
† These authors contributed equally to this work.

Abstract: Renal pathophysiology is a multifactorial process involving different kidney structures. Acute kidney injury (AKI) is a clinical condition characterized by tubular necrosis and glomerular hyperfiltration. The maladaptive repair after AKI predisposes to the onset of chronic kidney diseases (CKD). CKD is a progressive and irreversible loss of kidney function, characterized by fibrosis that could lead to end stage renal disease. In this review we provide a comprehensive overview of the most recent scientific publications analyzing the therapeutic potential of Extracellular Vesicles (EV)-based treatments in different animal models of AKI and CKD. EVs from multiple sources act as paracrine effectors involved in cell-cell communication with pro-generative and low immunogenic properties. They represent innovative and promising natural drug delivery vehicles used to treat experimental acute and chronic kidney diseases. Differently from synthetic systems, EVs can cross biological barriers and deliver biomolecules to the recipient cells inducing a physiological response. Moreover, new methods for improving the EVs as carriers have been introduced, such as the engineering of the cargo, the modification of the proteins on the external membrane, or the pre-conditioning of the cell of origin. The new nano-medicine approaches based on bioengineered EVs are an attempt to enhance their drug delivery capacity for potential clinical applications.

Figure 17. Abstract of the paper Ceccotti E. Saccu G. et al. Naïve or Engineered Extracellular Vesicles from Different Cell Sources: Therapeutic Tools for Kidney Diseases. Pharm. 2023. DOI: https://doi.org/10.3390/pharmaceutics15061715.

The other one speculates the application of extracellular vesicles as a potential biomarker for chronic liver diseases evaluating non-coding RNAs (Figure 18).

biomolecules

MDPI

Review

Extracellular Vesicles as Delivery Vehicles for Non-Coding RNAs: Potential Biomarkers for Chronic Liver Diseases

Arianna Ferro [1], Gabriele Saccu [1], Simone Mattivi [1], Andrea Gaido [1], Maria Beatriz Herrera Sanchez [2,3], Shafiul Haque [4,5,6], Lorenzo Silengo [3], Fiorella Altruda [3], Marilena Durazzo [1] and Sharmila Fagoonee [7,*]

1 Department of Medical Sciences, University of Turin, 10126 Turin, Italy; arianna.ferro@unito.it (A.F.); gabriele.saccu@unito.it (G.S.); simone.mattivi@unito.it (S.M.); andrea.gaido@unito.it (A.G.); marilena.durazzo@unito.it (M.D.)
2 2i3T, Società per la Gestione Dell'incubatore di Imprese e per il Trasferimento Tecnologico, University of Torino, 10126 Turin, Italy; maria.herrera@2i3t.it or mariabeatriz.herrera@unito.it
3 Molecular Biotechnology Centre "Guido Tarone", 10126 Turin, Italy; lorenzo.silengo@unito.it (L.S.); fiorella.altruda@unito.it (F.A.)
4 Research and Scientific Studies Unit, College of Nursing and Health Sciences, Jazan University, Jazan 45142, Saudi Arabia; shafiul.haque@hotmail.com
5 Centre of Medical and Bio-Allied Health Sciences Research, Ajman University, Ajman 13306, United Arab Emirates
6 Gilbert and Rose-Marie Chagoury School of Medicine, Lebanese American University, Beirut 1102 2801, Lebanon
7 Institute for Biostructure and Bioimaging, National Research Council (CNR), Molecular Biotechnology Centre "Guido Tarone", 10126 Turin, Italy
* Correspondence: sharmila.fagoonee@unito.it; Tel.: +39-0116706423

Abstract: In recent years, EVs have emerged as promising vehicles for coding and non-coding RNAs (ncRNAs), which have demonstrated remarkable potential as biomarkers for various diseases, including chronic liver diseases (CLDs). EVs are small, membrane-bound particles released by cells, carrying an arsenal of ncRNAs, including microRNAs (miRNAs), long non-coding RNAs (lncRNAs), and other ncRNA species, such as piRNAs, circRNAs, and tsRNAs. These ncRNAs act as key regulators of gene expression, splicing, and translation, providing a comprehensive molecular snapshot of the cells of origin. The non-invasive nature of EV sampling, typically via blood or serum collection, makes them highly attractive candidates for clinical biomarker applications. Moreover, EV-encapsulated ncRNAs offer unique advantages over traditional cell-free ncRNAs due to their enhanced stability within the EVs, hence allowing for their detection in circulation for extended periods and enabling more sensitive and reliable biomarker measurements. Numerous studies have investigated the potential of EV-enclosed ncRNAs as biomarkers for CLD. MiRNAs, in particular, have gained significant attention due to their ability to rapidly respond to changes in cellular stress and inflammation, hallmarks of CLD pathogenesis. Elevated levels of specific miRNAs have been consistently associated with various CLD subtypes, including metabolic dysfunction-associated steatotic liver disease (MASLD), metabolic dysfunction-associated steatohepatitis (MASH), and chronic hepatitis B and C. LncRNAs have also emerged as promising biomarkers for CLD. These transcripts are involved in a wide range of cellular processes, including liver regeneration, fibrosis, and cancer progression. Studies have shown that lncRNA expression profiles can distinguish between different CLD subtypes, providing valuable insights into disease progression and therapeutic response. Promising EV-enclosed ncRNA biomarkers for CLD included miR-122 (elevated levels of miR-122 are associated with MASLD progression and liver fibrosis), miR-21 (increased expression of miR-21 is linked to liver inflammation and fibrosis in CLD patients), miR-192 (elevated levels of miR-192 are associated with more advanced stages of CLD, including cirrhosis and HCC), LncRNA HOTAIR (increased HOTAIR expression is associated with MASLD progression and MASH development), and LncRNA H19 (dysregulation of H19 expression is linked to liver fibrosis and HCC progression). In the present review, we focus on the EV-enclosed ncRNAs as promising tools for the diagnosis and monitoring of CLD of various etiologies.

check for updates

Citation: Ferro, A.; Saccu, G.; Mattivi, S.; Gaido, A.; Herrera Sanchez, M.B.; Haque, S.; Silengo, L.; Altruda, F.; Durazzo, M.; Fagoonee, S. Extracellular Vesicles as Delivery Vehicles for Non-Coding RNAs: Potential Biomarkers for Chronic Liver Diseases. *Biomolecules* **2024**, *14*, 277. https://doi.org/10.3390/biom14030277

Academic Editor: William Cho

Received: 20 December 2023
Revised: 15 February 2024
Accepted: 21 February 2024
Published: 26 February 2024

Figure 18. Abstract of the paper Ferro A. et al Extracellular Vesicles as Delivery Vehicles for Non-Coding RNAs: Potential Biomarkers for Chronic Liver Diseases. Biomolecules. 2024 Feb 26;14(3):277. doi: 10.3390/biom14030277

The other one speculates the emerging and innovating cancer immunotherapies, especially in solid tumor (Figure 19).

Open Access Review

Emerging Cancer Immunotherapies: Cutting-Edge Advances and Innovations in Development

by Monica Maccagno [1,2,*], Marta Tapparo [2,3], Gabriele Saccu [2,3], Letizia Rumiano [1,2], Sharad Kholia [2,3], Lorenzo Silengo [2] and Maria Beatriz Herrera Sanchez [2,4,*]

[1] Department of Molecular Biotechnology and Health Sciences, 10126 Turin, Italy
[2] Molecular Biotechnology Centre, University of Torino, 10126 Turin, Italy
[3] Department of Medical Sciences, University of Torino, 10126 Turin, Italy
[4] 2i3T, Società per la Gestione dell'incubatore di Imprese e per il Trasferimento Tecnologico, University of Torino, 10126 Turin, Italy
[*] Authors to whom correspondence should be addressed.

Med. Sci. **2024**, *12*(3), 43; **https://doi.org/10.3390/medsci12030043**

Submission received: 11 July 2024 / Revised: 8 August 2024 / Accepted: 22 August 2024 / Published: 28 August 2024

Download Browse Figures Review Reports Versions Notes

Abstract

The rise in biological therapies has revolutionized oncology, with immunotherapy leading the charge through breakthroughs such as CAR-T cell therapy for melanoma and B-ALL. Modified bispecific antibodies and CAR-T cells are being developed to enhance their effectiveness further. However, CAR-T cell therapy currently relies on a costly ex vivo manufacturing process, necessitating alternative strategies to overcome this bottleneck. Targeted in vivo viral transduction offers a promising avenue but remains under-optimized. Additionally, novel approaches are emerging, such as in vivo vaccine boosting of CAR-T cells to strengthen the immune response against tumors, and dendritic cell-based vaccines are under investigation. Beyond CAR-T cells, mRNA therapeutics represent another promising avenue. Targeted delivery of DNA/RNA using lipid nanoparticles (LNPs) shows potential, as LNPs can be directed to T cells. Moreover, CRISPR editing has demonstrated the ability to precisely edit the genome, enhancing the effector function and persistence of synthetic T cells. Enveloped delivery vehicles packaging Cas9 directed to modified T cells offer a virus-free method for safe and effective molecule release. While this platform still relies on ex vivo transduction, using cells from healthy donors or induced pluripotent stem cells can reduce costs, simplify manufacturing, and expand treatment to patients with low-quality T cells. The use of allogeneic CAR-T cells in cancer has gained attraction for its potential to lower costs and broaden accessibility. This review emphasizes critical strategies for improving the selectivity and efficacy of immunotherapies, paving the way for a more targeted and successful fight against cancer.

Keywords: immunotherapy; cell therapy; cancer; CAR-T; CRISPR/Cas9; LNPs; vaccine

Figure 19. Abstract of the paper Maccagno M, Tapparo M, Saccu G, et al. Emerging Cancer Immunotherapies: Cutting-Edge Advances and Innovations in Development. *Med Sci (Basel)*. 2024;12(3):43. Published 2024 Aug 28. doi:10.3390/medsci12030043

Appendix 2

During my PhD, I had the opportunity to take part in different national and international conferences. The following is the oral communication I have presented:

EVIta Workshop "EV Connect: fostering collaboration" (Torino, September 2022). Abstract title: Bone Marrow Mesenchymal Stromal/Stem Cell-Derived Extracellular Vesicles Promote Corneal Wound Repair by Regulating Inflammation and Angiogenesis".

Abroad Period

During last 10 month of my PhD program, I had the opportunity to join the lab of Professor Chiarle at Boston children's hospital (BCH), Harvard medical school (HMS). Here, my study was based and focused on a different field- immunotherapy- that encompass cell therapy, employing chimeric antigen receptor (CAR)-T and T cell receptor (TCR)-T strategy in order to target anaplastic lymphoma kinase (ALK) positive tumor. In particular, I investigated combination of both therapy in neuroblastoma (NB) and Merkel cell carcinoma (MCC) ALK + solid tumor models.

ALK was reported for the first time in 1994 as the NPM-ALK fusion protein, expressed in most anaplastic large T-cell lymphomas (ALCL). ALK is a receptor protein-tyrosine kinase, a member of the insulin receptor superfamily, which is physiologically involved in the development of the embryonic nervous system. Furthermore, aberrant ALK activation has been identified such as ALK gain-of-function mutations, and ALK amplification [75]. Several ALK-fusion proteins have been described as a chromosomal rearrangement each implicated in different cancers such as ALCL, diffuse large B-cell lymphoma, inflammatory myofibroblastic tumors (IMT) [76]. Moreover, EML4-ALK fusion protein contribute to about 5% of non-small cell lung cancers (NSCLC). Notably, the N-terminal portion of these fusion proteins facilitates dimerization, which crucially activates the tumorigenic kinase domain of ALK. ALK fusion proteins trigger downstream signaling pathways that promote cancer cell growth and proliferation activating Ras/Raf/MEK/ERK1/2 and survival

pathway trough JAK/STAT [76] . Additionally, activating mutations and overexpression of ALK both contribute to the development of childhood neuroblastoma [77].

The discovery of oncogenic ALK alterations, particularly in non-small cell lung cancer (NSCLC) and lymphoma, has fueled significant research efforts to develop strategies for inhibiting ALK. Tyrosine kinase inhibitors (TKIs) represent a major breakthrough with the approval by the US Food and Drug Administration (FDA) for the treatment of ALK-positive NSCLC, ALCL, and other malignancies [78]. The first-generation TKI, crizotinib, revolutionized therapy for ALK+ tumors. However, the emergence of resistance necessitated the development of second- and third- generation TKIs with improved efficacy, such as brigatinib, alectinib, ceritinib, and lorlatinib [76,79] . Nonetheless, in ALK+ tumors drug resistance develops invariably, prompting the development of new strategies to eradicate disease such as immunotherapy. The field of cancer immunotherapy is rapidly evolving, with researchers investigating promising approaches such as cancer vaccines, immune checkpoint inhibitors (ICIs), CAR-T cells, TCR-T cells, and tumor-infiltrating lymphocytes (TILs) [80].

CAR-T cell therapy has been demonstrating revolutionary impact in cancer treatment that harnesses the power of the immune system. It involves genetically modifying a patient's own T-cells, to express a chimeric antigen receptor (CAR). This engineered receptor allows the T-cells to specifically recognize and attack cancer cells. CAR-T therapy has shown indeed remarkable success in treating blood cancer against CD19 and BCMA molecule with several FDA approved clinical trial (NCT02228096; NCT02348216; NCT02601313; NCT02631044; NCT03361748; NCT03548207)[81]. Beyond CAR-T, since 2010, the development of armored CAR-T and TCR-T (T cell Receptor T cell) therapies has expanded the scope of genetically engineered T cell treatments for cancer. Autologous or allogeneic TCR-T cells can be engineered to express TCRs that recognize multiple combinations of specific peptides and human leukocyte antigens (HLA) through advancements in TCR isolation, sequencing, and genetic engineering techniques. Unlike CAR-T cells, which target antigens on the cell surface, TCR-T cells can recognize a broader range of tumor-

associated antigens, including those derived from intracellular proteins [82]. The advantages of TCR-T therapy include its high specificity for cancer cells, its ability to target a wider range of antigens, including intracellular ones, and its increased potential in treating solid tumors. TCR-T therapy is still largely in the experimental and clinical trial stages, but it has shown promise in treating various cancers, including melanoma and synovial sarcoma [83,84]. Nonetheless, acquired resistance develops within 2-3 years, highlighting the urgent need for novel and effective therapeutic strategies for these patients [80]. Indeed, tumor heterogenicity and resistance mechanism may lead to down-regulation of the target antigen, relevant for CAR-T therapy and HLA class I antigen presentation, respectively relevant for TCR-T cell therapy. HLA-I expression is universally present on nucleated cells but varies by tissue and cell type to regulate immune function. Several studies have shown a close relation between the interferon-γ (IFN-γ) response pathway and HLA-I expression, which lead and enhances T cell-mediated anti-tumor immunity [85].

In fetal development, selective downregulation of HLA-A and HLA-B promotes maternal tolerance. Similar HLA-I downregulation occurs in adult tissue-specific stem cells [86]. Burr et al demonstrated that resistance to cancer immunotherapies may occur through genomic mutations and epigenetic phenomenon that inactivate the HLA-I antigen presenting peptide [87]. These findings suggest conserved epigenetic mechanisms that suppress HLA-I, potentially aiding cancer cells in evading immune detection; especially in neuroblastoma, small cell lung cancer (SCLC) and Merkel cell carcinoma [30,88,89]. Together these studies emphasize the central importance of understanding the regulation of HLA-I antigen presentation in cancer cells to enable effective targeting with immunotherapy.

Nowadays, it has been investigated how to prevent immune escape mechanism such as use of drugs that stimulate immune- cancer axis and the combination of different immunotherapy strategies has further studied. Of note, combination of CAR and TCR-T technology has demonstrated being a valid strategy to prevent immune escape mechanism [87].

The laboratory of Prof. Chiarle has explored the potential of targeting ALK-positive tumors through immunotherapy. Indeed, ALK immunogenic properties were highlighted by different methods, including DNA and peptide vaccination, as well as chimeric antigen receptor (CAR) T-cell and T cell receptor T-cell therapy in various ALK+ malignancies [77,90-92]. Collectively, these findings strongly support that ALK is a particularly attractive target for immunotherapy therapeutic approach.

This study aims to develop a novel therapeutic approach for ALK+ tumors, such as neuroblastoma and Merkel cell carcinoma, which express the ALK receptor on their surface and exhibit low HLA class I expression. I propose a combination therapy using CAR-T and TCR-T cells. Furthermore, we hypothesize that IFN-γ released upon activation of ALK.CAR-T cells can upregulate HLA class I expression on tumor cells, thereby enhancing the killing activity of both ALK.CAR and ALK.TCR-T cells.

In order to set up in vitro model for the killing activity of CAR/TCR-T cell therapy , we first define different whether ALK + Neuroblastoma and Merkel cells express HLA complex and HLA-B*07 isotype on cell membrane surface in basal condition and upon IFN-γ stimulation.

I set up an in vitro model to evaluate if neuroblastoma cell lines and Merkel ALK+ cells expressed HLA class I – especially subtype HLA-B*07:02- in basal condition and after IFN-γ stimulation. As shown in figure 1, different doses of IFN-γ are able to induce HLA expression, confirmed by HLA-A/B/C FACS analysis. However, none of neuroblastoma cells express the HLA of interest. Among Merkel carcinoma cells, WaGa cells expressed HLA-B*07. Thus, I employee this cell line to preform future experiments.

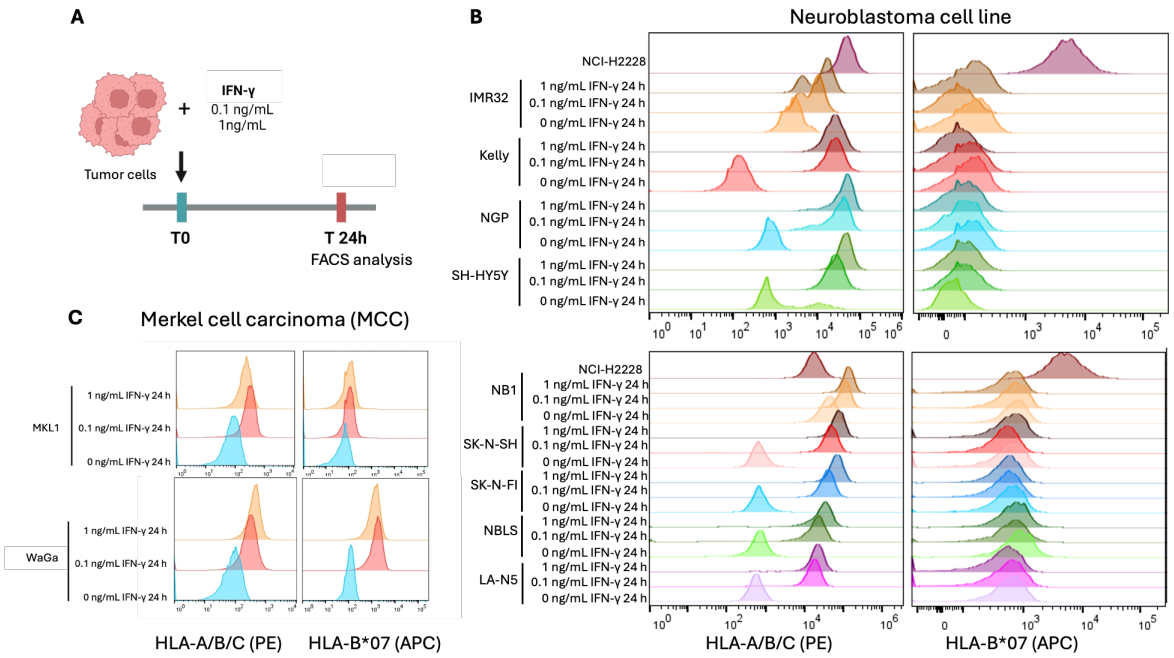

Figure 1: Screening of HLA class I induction in ALK+ tumor cell. (A) Schematic representation of IFN-Y in vitro assay using different tumor cell line. (B) FACS analysis of HLA-A/B/C and HLA-B*07 on Neuroblastoma cells line with different doses of IFN-γ. NCI-H2228 (non-small cell lung cancer) cell line was used as positive control. (C) FACS analysis of HLA-A/B/C and HLA-B*07 on Merkel carcinoma cells.

To further investigate the minimum effective dose for inducing HLA-I expression, we tested IFN-γ concentrations ranging from 0.01 to 1 ng/mL. FACS analysis revealed that all IFN-γ doses were able to upregulate MHC class I expression. Furthermore, RT-PCR confirmed the upregulation of key genes involved in HLA-I presentation, including TAP1, TAP2, hNLRC5, hB2m, HLA-A, and HLA-B (Figure 2).

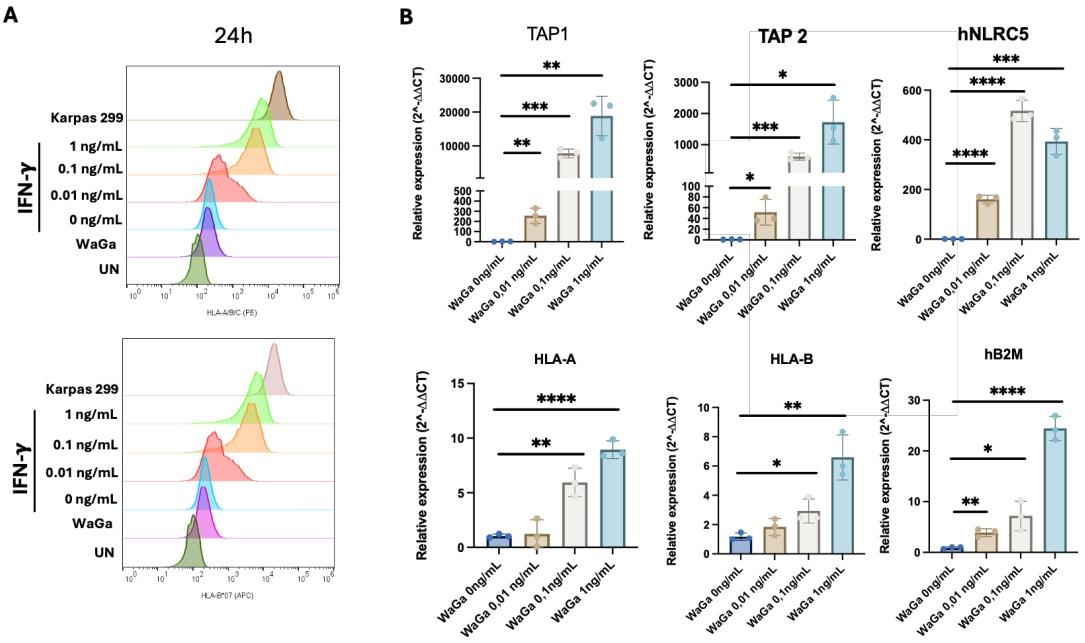

Figure 2: IFN-Y doses induce HLA-I induction in WaGa cell line. (A) FACS analysis with different doses of INF-Y on WaGa cell line. Karpas299 was used as positive control. (B) RT-PCR gene expression data of the key factor involved in HLA presentation. The results are presented as mean values of three independent experiments ±SD. *p < 0.05, **p <0.01, ***p <0.005, ****p <0.001 represent WaGa 0 ng/mL vs. WaGa 0.01 ng/mL; 0.1 ng/mL; and 1 ng/mL dose of IFN-γ.

Subsequentially, during my abroad period, I evaluated if IFN-γ released by ALK.CAR-T cell is able to indue HLA expression. In this phase, I generated ALK.CAR-T cell as previously described [77]. Briefly, The ALK.CAR cassettes were cloned into the retroviral vector encoding for human CD8a, CD28, and CD3z, and the ALK-scFv. For the preparation of retroviral supernatants used for the transduction of human T cells, 293T cells were transfected with the plasmid mixture of the retroviral vector. Supernatants containing the retrovirus were collected 48 hours after transfection. For the generation of engineered T cell, CD3+ T cells were isolated from peripheral blood, activated with Human T-Activator CD3/CD28 beads, and cultured with rhIL-7 and rhIL-15. After 2 days, CD3+ T cells were transduced with retroviral supernatants using retronectin-coated 24 multi/well plates. On day 12-14, cells are collected for in vitro experiments [77]. To investigate whether IFN-γ released by ALK.CAR-T cells could induce HLA expression, we co-cultured tumor cells with engineered T cells at various ratios (1:1 and 1:5 effector-to-target ratio - E:T). Conditioned media (CM) was then collected for further analysis. Two different assays were performed: quantification of IFN-Y and

stimulation of WaGa using CM. CD19.CAR-T cell were used as negative control. As shown in Figure 3A, ELISA analysis revealed significantly higher IFN-γ release during co-culture with ALK.CAR-T cells compared to CD19.CAR-T cell supernatant. Additionally, stimulation of WaGa cells with CM derived from ALK.CAR-T co-cultures induced HLA class I expression, particularly B*07, compared to CD19.CAR CM treatment. These results suggest that ALK.CAR-T cell co-culture with the specific target antigen leads to IFN-γ release, which induces HLA expression (Figure 3B).

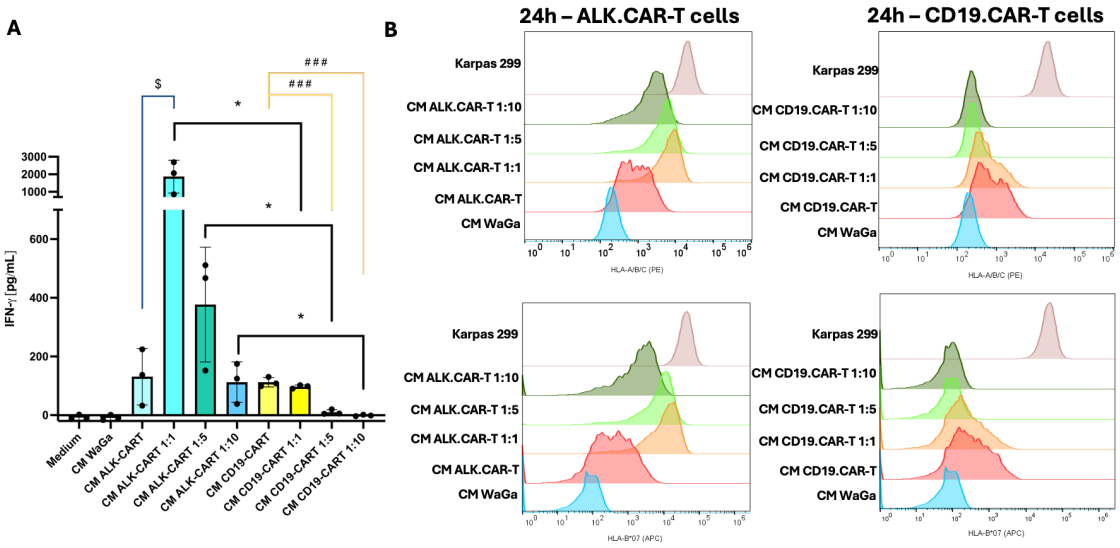

Figure 3: ALK.CAR-T cell released INF-Y stimulate HLA-I expression. **(A)** ELISA quantification of IFN-γ released in conditioned media by CAR-T cells after 24 h of co-culture with WaGa cells. The results are presented as mean values of three independent experiments ±SD.*$p < 0.05$ CM ALK.CAR-T 1:1 vs CM CD19.CAR-T 1:1; CM ALK.CAR-T 1:5 vs CM CD19.CAR-T 1:5; CM ALK.CAR-T 1:10 vs CM CD19.CAR-T 1:10. $^{\$}p < 0.05$ CM ALK.CAR-T vs CM ALK.CAR-T 1:1; $^{\#\#\#}p < 0.005$ CM CD19.CAR-T vs CM CD19.CAR-T 1:1, CM ALK.CAR-T 1:5 and CM CD19.CAR-T 1:10. **(B)** FACS analysis with different doses of CM in vitro WaGa cell model using ALK.CAR-T and CD19.CAR-t cells. Karpas299 was used as positive control.

During my last months at Chiarle lab, I first aimed to generate a single engineered T cell expressing both CAR and TCR molecules on its surface. ALK.CAR/TCR was produced using the same ALK.CAR-T cell protocol [77]. To investigate the positivity level for CAR, I employed Liker staining which is able to recognize a specific portion of scFv presented by ALK.CAR-T cells. On the other hand, dextramer staining was used to detect TCR compound. Dextramer is MHC-fluorophore complex attached to a dextran backbone molecule that is able to bind a specific TCR expressed on the surface of the cell. As shown in Figure 4A, FACS analysis of isolated CD8+ T cells revealed

double positivity for both the CAR construct and the TCR receptor, confirmed by linker and Dextramer staining, respectively. Notably, 72.2% of CD8+ T cells were co-infected with both constructs, demonstrating high infection efficiency. We then validated the killing capabilities of ALK.CAR/TCR cells against various cell lines, including NB1 (ALK-amplified), NCI-H2228 (ALK-fused with HLA-B07:02), NCI-H3122 (ALK-fused but HLA-B*07:02 negative), and WaGa (ALK wild-type with HLA-B*07:02). Figure 4B demonstrates the specific killing activity of ALK.CAR/TCR cells compared to single treatments (ALK.CAR-T or ALK.TCR-T alone) at E:T ratios (1:1 and 1:5). Additionally, we investigated the efficacy of combining ALK.CAR and ALK.TCR-T cells in a 1:1 ratio within different tumor models.

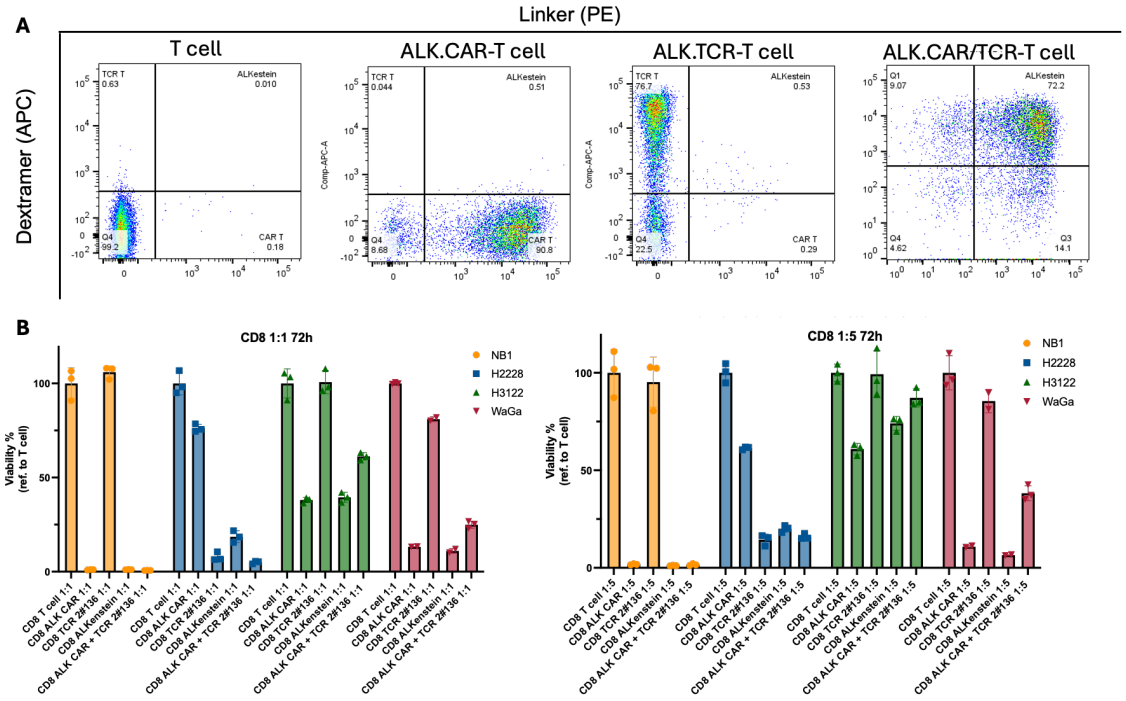

Figure 4: ALK.CAR/TCR-T cell validation. (A) FASC analysis of T cell; ALK.CAR; ALK.TCR and ALK.CAR/TCR- CD8+ T cell. (B) Killing co-culture assay of NB1(orange), NCI-H2228(blue), NCI-H3122 (green) and WaGa (red) tumoral cell line treated with T cell; ALK.CAR; ALK.TCR; ALK.CAR/TCR- cell and 1:1 ALK.CAR+ALK.TCR- CD8+ T. The results are presented percentage of total viability as mean values of three technical replicates ±SD. All data are normalized referring to T cell.

This study demonstrates that CAR-T therapy can induce first HLA expression by releasing IFN-γ, upregulating the gene signature of HLA class I. Additionally, engineered T cells co-expressing CAR and TCR on their surface are capable of killing tumor cell lines. These findings suggest that combining CAR and TCR molecules into the same cell could be a novel approach to treating ALK+ tumors by targeting surface antigens and inducing HLA class I expression, which can be targeted by TCR compounds.

This educational experience has provided me with a valuable opportunity to deepen my understanding of cell therapy from an immunological perspective. Notably, the use of immunotherapy, which integrates both gene and cell therapy, has expanded beyond oncology and is now positioned to address a wider range of conditions. Advances in CAR design and delivery technologies further enhance this potential, with promising applications in treating autoimmune diseases, fibrosis (heart and liver), and cellular senescence, as well as promoting healthy aging[93]. In a innovative study, CAR-T cells have been generated directly within the body to generate anti- fibrotic CAR-T cardiac fibrosis. Researchers utilized lipid nanoparticles (LNPs) targeted to T cells to deliver modified mRNA encoding chimeric antigen receptors (CARs). These transient CAR T cells selectively eliminated activated cardiac fibroblasts in a mouse model of heart failure, reducing fibrosis and improving cardiac function [94].

Recently, Amor et al, evaluated the senolytic ability of urokinase-type plasminogen activator receptor (uPAR)-CAR T cells to specifically ablate senescent cells in vitro and in vivo. Their results showed an efficient elimination of senescent cells and the further combination of CAR-T with senescence inducing agents (MEK and CDK4/6 inhibitors) much improved treatment outcome and such combinatorial strategies could be used against solid tumors. Additionally, the authors explored the applications of senolytic CAR T cells in the treatment of other senescence-related disorders, such as liver fibrosis. Thus, m.uPAR-m.28z CAR T were employed in CCl4-induced and non-alcoholic

steatohepatitis (NASH)-induced liver fibrosis were chosen as two models of chronic tissue pathologies showing a remarkable efficacy eliminating senescent cells, reduce fibrosis, and improve liver function [95]. Overall, several studies have been demonstrating and will display the ability of immunotherapy as valid and pivotal strategy not only for treating cancer (hematological and solid malignancies), but to embrace and treat different other diseases not cancer related.

References

1. Devarbhavi, H.; Asrani, S.K.; Arab, J.P.; Nartey, Y.A.; Pose, E.; Kamath, P.S. Global burden of liver disease: 2023 update. *J Hepatol* **2023**, *79*, 516-537, doi:10.1016/j.jhep.2023.03.017.
2. Weiler, N.; Schlotmann, A.; Schnitzbauer, A.A.; Zeuzem, S.; Welker, M.W. The Epidemiology of Acute Liver Failure. *Dtsch Arztebl Int* **2020**, *117*, 43-50, doi:10.3238/arztebl.2020.0043.
3. Vacanti, J.P.; Kulig, K.M. Liver cell therapy and tissue engineering for transplantation. *Semin Pediatr Surg* **2014**, *23*, 150-155, doi:10.1053/j.sempedsurg.2014.05.001.
4. Hoang, D.M.; Pham, P.T.; Bach, T.Q.; Ngo, A.T.L.; Nguyen, Q.T.; Phan, T.T.K.; Nguyen, G.H.; Le, P.T.T.; Hoang, V.T.; Forsyth, N.R.; et al. Stem cell-based therapy for human diseases. *Signal Transduct Target Ther* **2022**, *7*, 272, doi:10.1038/s41392-022-01134-4.
5. Tsolaki, E.; Yannaki, E. Stem cell-based regenerative opportunities for the liver: State of the art and beyond. *World J Gastroenterol* **2015**, *21*, 12334-12350, doi:10.3748/wjg.v21.i43.12334.
6. Liu, P.; Mao, Y.; Xie, Y.; Wei, J.; Yao, J. Stem cells for treatment of liver fibrosis/cirrhosis: clinical progress and therapeutic potential. *Stem Cell Res Ther* **2022**, *13*, 356, doi:10.1186/s13287-022-03041-5.
7. Li, Y.; Lu, L.; Cai, X. Liver Regeneration and Cell Transplantation for End-Stage Liver Disease. *Biomolecules* **2021**, *11*, doi:10.3390/biom11121907.
8. Pareja, E.; Gómez-Lechón, M.J.; Tolosa, L. Induced pluripotent stem cells for the treatment of liver diseases: challenges and perspectives from a clinical viewpoint. *Ann Transl Med* **2020**, *8*, 566, doi:10.21037/atm.2020.02.164.
9. Thanaskody, K.; Jusop, A.S.; Tye, G.J.; Wan Kamarul Zaman, W.S.; Dass, S.A.; Nordin, F. MSCs vs. iPSCs: Potential in therapeutic applications. *Front Cell Dev Biol* **2022**, *10*, 1005926, doi:10.3389/fcell.2022.1005926.
10. Lagasse, E.; Connors, H.; Al-Dhalimy, M.; Reitsma, M.; Dohse, M.; Osborne, L.; Wang, X.; Finegold, M.; Weissman, I.L.; Grompe, M. Purified hematopoietic stem cells can differentiate into hepatocytes in vivo. *Nat Med* **2000**, *6*, 1229-1234, doi:10.1038/81326.
11. Alison, M.R.; Poulsom, R.; Jeffery, R.; Dhillon, A.P.; Quaglia, A.; Jacob, J.; Novelli, M.; Prentice, G.; Williamson, J.; Wright, N.A. Hepatocytes from non-hepatic adult stem cells. *Nature* **2000**, *406*, 257, doi:10.1038/35018642.
12. Petersen, B.E.; Bowen, W.C.; Patrene, K.D.; Mars, W.M.; Sullivan, A.K.; Murase, N.; Boggs, S.S.; Greenberger, J.S.; Goff, J.P. Bone marrow as a potential source of hepatic oval cells. *Science* **1999**, *284*, 1168-1170, doi:10.1126/science.284.5417.1168.
13. Pai, M.; Zacharoulis, D.; Milicevic, M.N.; Helmy, S.; Jiao, L.R.; Levicar, N.; Tait, P.; Scott, M.; Marley, S.B.; Jestice, K.; et al. Autologous infusion of expanded mobilized adult bone marrow-derived CD34+ cells into patients with alcoholic liver cirrhosis. *Am J Gastroenterol* **2008**, *103*, 1952-1958, doi:10.1111/j.1572-0241.2008.01993.x.

14. Han, Y.; Yan, L.; Han, G.; Zhou, X.; Hong, L.; Yin, Z.; Zhang, X.; Wang, S.; Wang, J.; Sun, A.; et al. Controlled trials in hepatitis B virus-related decompensate liver cirrhosis: peripheral blood monocyte transplant versus granulocyte-colony-stimulating factor mobilization therapy. *Cytotherapy* **2008**, *10*, 390-396, doi:10.1080/14653240802129901.
15. Thorgeirsson, S.S.; Grisham, J.W. Hematopoietic cells as hepatocyte stem cells: a critical review of the evidence. *Hepatology* **2006**, *43*, 2-8, doi:10.1002/hep.21015.
16. Han, Y.; Li, X.; Zhang, Y.; Chang, F.; Ding, J. Mesenchymal Stem Cells for Regenerative Medicine. *Cells* **2019**, *8*, doi:10.3390/cells8080886.
17. Berardis, S.; Dwisthi Sattwika, P.; Najimi, M.; Sokal, E.M. Use of mesenchymal stem cells to treat liver fibrosis: current situation and future prospects. *World J Gastroenterol* **2015**, *21*, 742-758, doi:10.3748/wjg.v21.i3.742.
18. Liu, W.H.; Song, F.Q.; Ren, L.N.; Guo, W.Q.; Wang, T.; Feng, Y.X.; Tang, L.J.; Li, K. The multiple functional roles of mesenchymal stem cells in participating in treating liver diseases. *J Cell Mol Med* **2015**, *19*, 511-520, doi:10.1111/jcmm.12482.
19. Zhang, Z.H.; Zhu, W.; Ren, H.Z.; Zhao, X.; Wang, S.; Ma, H.C.; Shi, X.L. Mesenchymal stem cells increase expression of heme oxygenase-1 leading to anti-inflammatory activity in treatment of acute liver failure. *Stem Cell Res Ther* **2017**, *8*, 70, doi:10.1186/s13287-017-0524-3.
20. Wang, Y.H.; Wu, D.B.; Chen, B.; Chen, E.Q.; Tang, H. Progress in mesenchymal stem cell-based therapy for acute liver failure. *Stem Cell Res Ther* **2018**, *9*, 227, doi:10.1186/s13287-018-0972-4.
21. Driscoll, J.; Patel, T. The mesenchymal stem cell secretome as an acellular regenerative therapy for liver disease. *J Gastroenterol* **2019**, *54*, 763-773, doi:10.1007/s00535-019-01599-1.
22. Herrera, M.B.; Bruno, S.; Buttiglieri, S.; Tetta, C.; Gatti, S.; Deregibus, M.C.; Bussolati, B.; Camussi, G. Isolation and characterization of a stem cell population from adult human liver. *Stem Cells* **2006**, *24*, 2840-2850, doi:10.1634/stemcells.2006-0114.
23. Bruno, S.; Grange, C.; Tapparo, M.; Pasquino, C.; Romagnoli, R.; Dametto, E.; Amoroso, A.; Tetta, C.; Camussi, G. Human Liver Stem Cells Suppress T-Cell Proliferation, NK Activity, and Dendritic Cell Differentiation. *Stem Cells Int* **2016**, *2016*, 8468549, doi:10.1155/2016/8468549.
24. Herrera, M.B.; Fonsato, V.; Bruno, S.; Grange, C.; Gilbo, N.; Romagnoli, R.; Tetta, C.; Camussi, G. Human liver stem cells improve liver injury in a model of fulminant liver failure. *Hepatology* **2013**, *57*, 311-319, doi:10.1002/hep.25986.
25. Bruno, S.; Herrera Sanchez, M.B.; Pasquino, C.; Tapparo, M.; Cedrino, M.; Tetta, C.; Camussi, G. Human Liver-Derived Stem Cells Improve Fibrosis and Inflammation Associated with Nonalcoholic Steatohepatitis. *Stem Cells Int* **2019**, *2019*, 6351091, doi:10.1155/2019/6351091.
26. Bruno, S.; Pasquino, C.; Herrera Sanchez, M.B.; Tapparo, M.; Figliolini, F.; Grange, C.; Chiabotto, G.; Cedrino, M.; Deregibus, M.C.; Tetta, C.; et al. HLSC-Derived Extracellular Vesicles Attenuate Liver Fibrosis and Inflammation in a Murine Model of Non-alcoholic Steatohepatitis. *Mol Ther* **2020**, *28*, 479-489, doi:10.1016/j.ymthe.2019.10.016.

27. Spada, M.; Porta, F.; Righi, D.; Gazzera, C.; Tandoi, F.; Ferrero, I.; Fagioli, F.; Sanchez, M.B.H.; Calvo, P.L.; Biamino, E.; et al. Intrahepatic Administration of Human Liver Stem Cells in Infants with Inherited Neonatal-Onset Hyperammonemia: A Phase I Study. *Stem Cell Rev Rep* **2020**, *16*, 186-197, doi:10.1007/s12015-019-09925-z.
28. Prior, N.; Inacio, P.; Huch, M. Liver organoids: from basic research to therapeutic applications. *Gut* **2019**, *68*, 2228-2237, doi:10.1136/gutjnl-2019-319256.
29. Ober, E.A.; Lemaigre, F.P. Development of the liver: Insights into organ and tissue morphogenesis. *J Hepatol* **2018**, *68*, 1049-1062, doi:10.1016/j.jhep.2018.01.005.
30. Abdul-Al, M.; Kyeremeh, G.K.; Saeinasab, M.; Heidari Keshel, S.; Sefat, F. Stem Cell Niche Microenvironment: Review. *Bioengineering (Basel)* **2021**, *8*, doi:10.3390/bioengineering8080108.
31. Luo, Q.; Wang, N.; Que, H.; Mai, E.; Hu, Y.; Tan, R.; Gu, J.; Gong, P. Pluripotent Stem Cell-Derived Hepatocyte-like Cells: Induction Methods and Applications. *Int J Mol Sci* **2023**, *24*, doi:10.3390/ijms241411592.
32. Xie, Y.; Yao, J.; Jin, W.; Ren, L.; Li, X. Induction and Maturation of Hepatocyte-Like Cells. *Front Cell Dev Biol* **2021**, *9*, 765980, doi:10.3389/fcell.2021.765980.
33. Bertero, A.; Madrigal, P.; Galli, A.; Hubner, N.C.; Moreno, I.; Burks, D.; Brown, S.; Pedersen, R.A.; Gaffney, D.; Mendjan, S.; et al. Activin/nodal signaling and NANOG orchestrate human embryonic stem cell fate decisions by controlling the H3K4me3 chromatin mark. *Genes Dev* **2015**, *29*, 702-717, doi:10.1101/gad.255984.114.
34. Hannoun, Z.; Steichen, C.; Dianat, N.; Weber, A.; Dubart-Kupperschmitt, A. The potential of induced pluripotent stem cell derived hepatocytes. *J Hepatol* **2016**, *65*, 182-199, doi:10.1016/j.jhep.2016.02.025.
35. Snykers, S.; De Kock, J.; Tamara, V.; Rogiers, V. Hepatic differentiation of mesenchymal stem cells: in vitro strategies. *Methods Mol Biol* **2011**, *698*, 305-314, doi:10.1007/978-1-60761-999-4_23.
36. Underhill, G.H.; Khetani, S.R. Bioengineered Liver Models for Drug Testing and Cell Differentiation Studies. *Cell Mol Gastroenterol Hepatol* **2018**, *5*, 426-439.e421, doi:10.1016/j.jcmgh.2017.11.012.
37. Serras, A.S.; Rodrigues, J.S.; Cipriano, M.; Rodrigues, A.V.; Oliveira, N.G.; Miranda, J.P. A Critical Perspective on 3D Liver Models for Drug Metabolism and Toxicology Studies. *Front Cell Dev Biol* **2021**, *9*, 626805, doi:10.3389/fcell.2021.626805.
38. Khetani, S.R.; Bhatia, S.N. Microscale culture of human liver cells for drug development. *Nat Biotechnol* **2008**, *26*, 120-126, doi:10.1038/nbt1361.
39. Lauschke, V.M.; Hendriks, D.F.; Bell, C.C.; Andersson, T.B.; Ingelman-Sundberg, M. Novel 3D Culture Systems for Studies of Human Liver Function and Assessments of the Hepatotoxicity of Drugs and Drug Candidates. *Chem Res Toxicol* **2016**, *29*, 1936-1955, doi:10.1021/acs.chemrestox.6b00150.
40. Yiangou, L.; Ross, A.D.B.; Goh, K.J.; Vallier, L. Human Pluripotent Stem Cell-Derived Endoderm for Modeling Development and Clinical Applications. *Cell Stem Cell* **2018**, *22*, 485-499, doi:10.1016/j.stem.2018.03.016.

41. Gieseck, R.L.; Hannan, N.R.; Bort, R.; Hanley, N.A.; Drake, R.A.; Cameron, G.W.; Wynn, T.A.; Vallier, L. Maturation of induced pluripotent stem cell derived hepatocytes by 3D-culture. *PLoS One* **2014**, *9*, e86372, doi:10.1371/journal.pone.0086372.
42. Navran, S. The application of low shear modeled microgravity to 3-D cell biology and tissue engineering. *Biotechnol Annu Rev* **2008**, *14*, 275-296, doi:10.1016/S1387-2656(08)00011-2.
43. Chistiakov, D.A.; Chistiakov, P.A. Strategies to produce hepatocytes and hepatocyte-like cells from pluripotent stem cells. *Hepatol Res* **2012**, *42*, 111-119, doi:10.1111/j.1872-034X.2011.00896.x.
44. El-Hamid, S.A.; Mogawer, A. In vitro mesenchymal stem cells differentiation into hepatocyte-like cells in the presence and absence of 3D microenvironment.
45. Takebe, T.; Sekine, K.; Enomura, M.; Koike, H.; Kimura, M.; Ogaeri, T.; Zhang, R.R.; Ueno, Y.; Zheng, Y.W.; Koike, N.; et al. Vascularized and functional human liver from an iPSC-derived organ bud transplant. *Nature* **2013**, *499*, 481-484, doi:10.1038/nature12271.
46. Cipriano, M.; Freyer, N.; Knöspel, F.; Oliveira, N.G.; Barcia, R.; Cruz, P.E.; Cruz, H.; Castro, M.; Santos, J.M.; Zeilinger, K.; et al. Self-assembled 3D spheroids and hollow-fibre bioreactors improve MSC-derived hepatocyte-like cell maturation in vitro. *Arch Toxicol* **2017**, *91*, 1815-1832, doi:10.1007/s00204-016-1838-0.
47. Fonsato, V.; Herrera, M.B.; Buttiglieri, S.; Gatti, S.; Camussi, G.; Tetta, C. Use of a rotary bioartificial liver in the differentiation of human liver stem cells. *Tissue Eng Part C Methods* **2010**, *16*, 123-132, doi:10.1089/ten.TEC.2008.0634.
48. Navarro-Tableros, V.; Herrera Sanchez, M.B.; Figliolini, F.; Romagnoli, R.; Tetta, C.; Camussi, G. Recellularization of rat liver scaffolds by human liver stem cells. *Tissue Eng Part A* **2015**, *21*, 1929-1939, doi:10.1089/ten.TEA.2014.0573.
49. Elmaouhoub, A.; Dudas, J.; Ramadori, G. Kinetics of albumin- and alpha-fetoprotein-production during rat liver development. *Histochem Cell Biol* **2007**, *128*, 431-443, doi:10.1007/s00418-007-0338-y.
50. Barmore W, A.F., Stone WL. Physiology, Urea Cycle. **May 8, 2023 .**
51. Ah Mew N, S.K., Gropman AL, Lanpher BC, Chapman KA, Summar ML. Urea Cycle Disorders Overview. Adam MP, M.G., Pagon RA, Wallace SE, Bean LJH, Gripp KW, Amemiya A, Ed.; *GeneReviews*, 2003.
52. Soria, L.R.; Ah Mew, N.; Brunetti-Pierri, N. Progress and challenges in development of new therapies for urea cycle disorders. *Hum Mol Genet* **2019**, *28*, R42-R48, doi:10.1093/hmg/ddz140.
53. Herrera Sanchez, M.B.; Previdi, S.; Bruno, S.; Fonsato, V.; Deregibus, M.C.; Kholia, S.; Petrillo, S.; Tolosano, E.; Critelli, R.; Spada, M.; et al. Extracellular vesicles from human liver stem cells restore argininosuccinate synthase deficiency. *Stem Cell Res Ther* **2017**, *8*, 176, doi:10.1186/s13287-017-0628-9.
54. Takahashi, K.; Yamanaka, S. Induction of pluripotent stem cells from mouse embryonic and adult fibroblast cultures by defined factors. *Cell* **2006**, *126*, 663-676, doi:10.1016/j.cell.2006.07.024.

55. Ho, C.M.; Dhawan, A.; Hughes, R.D.; Lehec, S.C.; Puppi, J.; Philippeos, C.; Lee, P.H.; Mitry, R.R. Use of indocyanine green for functional assessment of human hepatocytes for transplantation. *Asian J Surg* **2012**, *35*, 9-15, doi:10.1016/j.asjsur.2012.04.017.

56. Schwarz, C.; Plass, I.; Fitschek, F.; Punzengruber, A.; Mittlböck, M.; Kampf, S.; Asenbaum, U.; Starlinger, P.; Stremitzer, S.; Bodingbauer, M.; et al. The value of indocyanine green clearance assessment to predict postoperative liver dysfunction in patients undergoing liver resection. *Sci Rep* **2019**, *9*, 8421, doi:10.1038/s41598-019-44815-x.

57. Kalliokoski, A.; Niemi, M. Impact of OATP transporters on pharmacokinetics. *Br J Pharmacol* **2009**, *158*, 693-705, doi:10.1111/j.1476-5381.2009.00430.x.

58. Saito, Y.; Ikemoto, T.; Morine, Y.; Shimada, M. Current status of hepatocyte-like cell therapy from stem cells. *Surg Today* **2021**, *51*, 340-349, doi:10.1007/s00595-020-02092-6.

59. Saito, M.; Matsuura, T.; Masaki, T.; Maehashi, H.; Shimizu, K.; Hataba, Y.; Iwahori, T.; Suzuki, T.; Braet, F. Reconstruction of liver organoid using a bioreactor. *World journal of gastroenterology : WJG* **2006**, *12*, 1881-1888.

60. Godoy, P.; Hewitt, N.J.; Albrecht, U.; Andersen, M.E.; Ansari, N.; Bhattacharya, S.; Bode, J.G.; Bolleyn, J.; Borner, C.; Böttger, J.; et al. Recent advances in 2D and 3D in vitro systems using primary hepatocytes, alternative hepatocyte sources and non-parenchymal liver cells and their use in investigating mechanisms of hepatotoxicity, cell signaling and ADME. *Arch Toxicol* **2013**, *87*, 1315-1530, doi:10.1007/s00204-013-1078-5.

61. Yamashita, T.; Takayama, K.; Sakurai, F.; Mizuguchi, H. Billion-scale production of hepatocyte-like cells from human induced pluripotent stem cells. *Biochem Biophys Res Commun* **2018**, *496*, 1269-1275, doi:10.1016/j.bbrc.2018.01.186.

62. Si-Tayeb, K.; Lemaigre, F.P.; Duncan, S.A. Organogenesis and development of the liver. *Dev Cell* **2010**, *18*, 175-189, doi:10.1016/j.devcel.2010.01.011.

63. Suominen, S.; Hyypijev, T.; Venäläinen, M.; Yrjänäinen, A.; Vuorenpää, H.; Lehti-Polojärvi, M.; Räsänen, M.; Seppänen, A.; Hyttinen, J.; Miettinen, S.; et al. Improvements in Maturity and Stability of 3D iPSC-Derived Hepatocyte-like Cell Cultures. *Cells* **2023**, *12*, doi:10.3390/cells12192368.

64. Miki, T.; Ring, A.; Gerlach, J. Hepatic differentiation of human embryonic stem cells is promoted by three-dimensional dynamic perfusion culture conditions. *Tissue Eng Part C Methods* **2011**, *17*, 557-568, doi:10.1089/ten.TEC.2010.0437.

65. McKee, C.; Chaudhry, G.R. Advances and challenges in stem cell culture. *Colloids Surf B Biointerfaces* **2017**, *159*, 62-77, doi:10.1016/j.colsurfb.2017.07.051.

66. Ogawa, S.; Surapisitchat, J.; Virtanen, C.; Ogawa, M.; Niapour, M.; Sugamori, K.S.; Wang, S.; Tamblyn, L.; Guillemette, C.; Hoffmann, E.; et al. Three-dimensional culture and cAMP signaling promote the maturation of human pluripotent stem cell-derived hepatocytes. *Development* **2013**, *140*, 3285-3296, doi:10.1242/dev.090266.

67. Mathieu, J.; Zhang, Z.; Nelson, A.; Lamba, D.A.; Reh, T.A.; Ware, C.; Ruohola-Baker, H. Hypoxia induces re-entry of committed cells into pluripotency. *Stem Cells* **2013**, *31*, 1737-1748, doi:10.1002/stem.1446.

68. Tsang, W.P.; Shu, Y.; Kwok, P.L.; Zhang, F.; Lee, K.K.; Tang, M.K.; Li, G.; Chan, K.M.; Chan, W.Y.; Wan, C. CD146+ human umbilical cord perivascular cells maintain stemness under hypoxia and as a cell source for skeletal regeneration. *PLoS One* **2013**, *8*, e76153, doi:10.1371/journal.pone.0076153.

69. Ahmed, N.E.; Murakami, M.; Kaneko, S.; Nakashima, M. The effects of hypoxia on the stemness properties of human dental pulp stem cells (DPSCs). *Sci Rep* **2016**, *6*, 35476, doi:10.1038/srep35476.

70. Gu, T.T.; Liu, S.Y.; Zheng, P.S. Cytoplasmic NANOG-positive stromal cells promote human cervical cancer progression. *Am J Pathol* **2012**, *181*, 652-661, doi:10.1016/j.ajpath.2012.04.008.

71. Topal, T.; Kim, B.C.; Villa-Diaz, L.G.; Deng, C.X.; Takayama, S.; Krebsbach, P.H. Rapid translocation of pluripotency-related transcription factors by external uniaxial forces. *Integr Biol (Camb)* **2019**, *11*, 41-52, doi:10.1093/intbio/zyz003.

72. Pradhan-Sundd, T.; Gudapati, S.; Kaminski, T.W.; Ragni, M.V. Exploring the Complex Role of Coagulation Factor VIII in Chronic Liver Disease. *Cell Mol Gastroenterol Hepatol* **2021**, *12*, 1061-1072, doi:10.1016/j.jcmgh.2021.02.014.

73. Sakka, S.G. Assessment of liver perfusion and function by indocyanine green in the perioperative setting and in critically ill patients. *J Clin Monit Comput* **2018**, *32*, 787-796, doi:10.1007/s10877-017-0073-4.

74. Lau, N.S.; Ly, M.; Liu, K.; Majumdar, A.; McCaughan, G.; Crawford, M.; Pulitano, C. Current and Potential Applications for Indocyanine Green in Liver Transplantation. *Transplantation* **2022**, *106*, 1339-1350, doi:10.1097/TP.0000000000004024.

75. Chiarle, R.; Voena, C.; Ambrogio, C.; Piva, R.; Inghirami, G. The anaplastic lymphoma kinase in the pathogenesis of cancer. *Nat Rev Cancer* **2008**, *8*, 11-23, doi:10.1038/nrc2291.

76. Roskoski, R. Anaplastic lymphoma kinase (ALK): structure, oncogenic activation, and pharmacological inhibition. *Pharmacol Res* **2013**, *68*, 68-94, doi:10.1016/j.phrs.2012.11.007.

77. Bergaggio, E.; Tai, W.T.; Aroldi, A.; Mecca, C.; Landoni, E.; Nüesch, M.; Mota, I.; Metovic, J.; Molinaro, L.; Ma, L.; et al. ALK inhibitors increase ALK expression and sensitize neuroblastoma cells to ALK.CAR-T cells. *Cancer Cell* **2023**, *41*, 2100-2116.e2110, doi:10.1016/j.ccell.2023.11.004.

78. Holla, V.R.; Elamin, Y.Y.; Bailey, A.M.; Johnson, A.M.; Litzenburger, B.C.; Khotskaya, Y.B.; Sanchez, N.S.; Zeng, J.; Shufean, M.A.; Shaw, K.R.; et al. ALK: a tyrosine kinase target for cancer therapy. *Cold Spring Harb Mol Case Stud* **2017**, *3*, a001115, doi:10.1101/mcs.a001115.

79. Desai, A.; Lovly, C.M. Strategies to overcome resistance to ALK inhibitors in non-small cell lung cancer: a narrative review. *Transl Lung Cancer Res* **2023**, *12*, 615-628, doi:10.21037/tlcr-22-708.

80. Zhang, Y.; Zhang, Z. The history and advances in cancer immunotherapy: understanding the characteristics of tumor-infiltrating immune cells and their therapeutic implications. *Cell Mol Immunol* **2020**, *17*, 807-821, doi:10.1038/s41423-020-0488-6.

81. Maccagno, M.; Tapparo, M.; Saccu, G.; Rumiano, L.; Kholia, S.; Silengo, L.; Herrera Sanchez, M.B. Emerging Cancer Immunotherapies: Cutting-Edge Advances and Innovations in Development. *Med Sci (Basel)* **2024**, *12*, doi:10.3390/medsci12030043.

82. Liu, Q.; Li, J.; Zheng, H.; Yang, S.; Hua, Y.; Huang, N.; Kleeff, J.; Liao, Q.; Wu, W. Adoptive cellular immunotherapy for solid neoplasms beyond CAR-T. *Mol Cancer* **2023**, *22*, 28, doi:10.1186/s12943-023-01735-9.

83. Yarza, R.; Bover, M.; Herrera-Juarez, M.; Rey-Cardenas, M.; Paz-Ares, L.; Lopez-Martin, J.A.; Haanen, J. Efficacy of T-Cell Receptor-Based Adoptive Cell Therapy in Cutaneous Melanoma: A Meta-Analysis. *Oncologist* **2023**, *28*, e406-e415, doi:10.1093/oncolo/oyad078.

84. Pan, Q.; Weng, D.; Liu, J.; Han, Z.; Ou, Y.; Xu, B.; Peng, R.; Que, Y.; Wen, X.; Yang, J.; et al. Phase 1 clinical trial to assess safety and efficacy of NY-ESO-1-specific TCR T cells in HLA-A∗02:01 patients with advanced soft tissue sarcoma. *Cell Rep Med* **2023**, *4*, 101133, doi:10.1016/j.xcrm.2023.101133.

85. Patel, S.J.; Sanjana, N.E.; Kishton, R.J.; Eidizadeh, A.; Vodnala, S.K.; Cam, M.; Gartner, J.J.; Jia, L.; Steinberg, S.M.; Yamamoto, T.N.; et al. Identification of essential genes for cancer immunotherapy. *Nature* **2017**, *548*, 537-542, doi:10.1038/nature23477.

86. Tilburgs, T.; Strominger, J.L. CD8+ effector T cells at the fetal-maternal interface, balancing fetal tolerance and antiviral immunity. *Am J Reprod Immunol* **2013**, *69*, 395-407, doi:10.1111/aji.12094.

87. Burr, M.L.; Sparbier, C.E.; Chan, K.L.; Chan, Y.C.; Kersbergen, A.; Lam, E.Y.N.; Azidis-Yates, E.; Vassiliadis, D.; Bell, C.C.; Gilan, O.; et al. An Evolutionarily Conserved Function of Polycomb Silences the MHC Class I Antigen Presentation Pathway and Enables Immune Evasion in Cancer. *Cancer Cell* **2019**, *36*, 385-401.e388, doi:10.1016/j.ccell.2019.08.008.

88. Bernards, R.; Dessain, S.K.; Weinberg, R.A. N-myc amplification causes down-modulation of MHC class I antigen expression in neuroblastoma. *Cell* **1986**, *47*, 667-674, doi:10.1016/0092-8674(86)90509-x.

89. Restifo, N.P.; Esquivel, F.; Kawakami, Y.; Yewdell, J.W.; Mulé, J.J.; Rosenberg, S.A.; Bennink, J.R. Identification of human cancers deficient in antigen processing. *J Exp Med* **1993**, *177*, 265-272, doi:10.1084/jem.177.2.265.

90. Chiarle, R.; Martinengo, C.; Mastini, C.; Ambrogio, C.; D'Escamard, V.; Forni, G.; Inghirami, G. The anaplastic lymphoma kinase is an effective oncoantigen for lymphoma vaccination. *Nat Med* **2008**, *14*, 676-680, doi:10.1038/nm1769.

91. Mota, I.; Patrucco, E.; Mastini, C.; Mahadevan, N.R.; Thai, T.C.; Bergaggio, E.; Cheong, T.C.; Leonardi, G.; Karaca-Atabay, E.; Campisi, M.; et al. ALK peptide vaccination restores the immunogenicity of ALK-rearranged non-small cell lung cancer. *Nat Cancer* **2023**, *4*, 1016-1035, doi:10.1038/s43018-023-00591-2.

92. Carmen, M.; Ana, A.; Luca, A.; Bergaggio, E.; Simone, P.; Marcos, S.-C.; L., R.E.; Rafael, B.-P.; Roberto, C. Discovery of ALK-specific TCR clonotypes for the development of TCR-T cell therapies against ALK-positive cancers. . **2024**, *84 (6_Supplement): 21*.
93. Baker, D.J.; Arany, Z.; Baur, J.A.; Epstein, J.A.; June, C.H. CAR T therapy beyond cancer: the evolution of a living drug. *Nature* **2023**, *619*, 707-715, doi:10.1038/s41586-023-06243-w.
94. Rurik, J.G.; Tombácz, I.; Yadegari, A.; Méndez Fernández, P.O.; Shewale, S.V.; Li, L.; Kimura, T.; Soliman, O.Y.; Papp, T.E.; Tam, Y.K.; et al. CAR T cells produced in vivo to treat cardiac injury. *Science* **2022**, *375*, 91-96, doi:10.1126/science.abm0594.
95. Amor, C.; Feucht, J.; Leibold, J.; Ho, Y.J.; Zhu, C.; Alonso-Curbelo, D.; Mansilla-Soto, J.; Boyer, J.A.; Li, X.; Giavridis, T.; et al. Senolytic CAR T cells reverse senescence-associated pathologies. *Nature* **2020**, *583*, 127-132, doi:10.1038/s41586-020-2403-9.

Acknowledgements

I would like to express my sincere gratitude to my supervisor, Professor Stefania Bruno, for her guidance and support throughout my research. Her extensive knowledge and experience were instrumental in the completion of my scientific journey and this dissertation.

I am also extremely thankful to my co-supervisor. Dr Maria Beatriz Herrera Sanchez. Her deep commitment to academic excellence and meticulous attention to detail have significantly shaped this dissertation and the final publication. Moreover, her insightful suggestions and encouragement inspire me over these years. Her critical question, comments and suggestions pushed me to sharp my thinking and brought greater depth to this work, and in general science.

It has been an amazing experience working also with Dr. Marta Tapparo, whose resources and assistance have been invaluable.

Special thanks to Professor Lorenzo Silengo, who generously provided knowledge and expertise. Additionally, this endeavor would not have been possible without the generous support from the "Fondazione per la Ricerca Biomedica (FORB)", who financed my research.

I would also like to acknowledge Professor Benedetta Bussolati, Dr. Sharmila Fagonee, Professor Roberto Chiarle and my peers for their stimulating discussions that inspired me throughout my academic journey. Their collective wisdom and encouragement have been a cornerstone of my research experience.